

**UNIVERSIDAD SAN FRANCISCO DE QUITO USFQ**

**Colegio de Posgrados**

**A Glitch in the Matrix: Phage predation dynamics in *Vibrio*-associated biofilms**

**Tesis en torno a una hipótesis o problema de investigación y su contrastación**

**Dario Fernando Cueva Granda**

**Antonio Machado, PhD.  
Director de Trabajo de Titulación**

Trabajo de titulación de posgrado presentado como requisito para la obtención del título de Magister en Microbiología

Quito, 22 de diciembre de 2023

**UNIVERSIDAD SAN FRANCISCO DE QUITO  
USFQ**

**COLEGIO DE POSGRADOS**

**HOJA DE APROBACIÓN DE TRABAJO DE TITULACIÓN**

**A Glitch in the Matrix: Phage predation dynamics in *Vibrio*-associated  
biofilms**

**Dario Fernando Cueva Granda**

Nombre del Director del Programa: Patricio Rojas Silva  
Título académico: M.D., PhD.  
Director del programa de: Maestría en Microbiología

Nombre del Decano del colegio Académico: Carlos Valle  
Título académico: PhD.  
Decano del Colegio: COCIBA

Nombre del Decano del Colegio de Posgrados: Hugo Burgos  
Título académico: PhD.

**Quito, 22 de diciembre 2023**

## © DERECHOS DE AUTOR

Por medio del presente documento certifico que he leído todas las Políticas y Manuales de la Universidad San Francisco de Quito USFQ, incluyendo la Política de Propiedad Intelectual USFQ, y estoy de acuerdo con su contenido, por lo que los derechos de propiedad intelectual del presente trabajo quedan sujetos a lo dispuesto en esas Políticas.

Asimismo, autorizo a la USFQ para que realice la digitalización y publicación de este trabajo en el repositorio virtual, de conformidad a lo dispuesto en la Ley Orgánica de Educación Superior del Ecuador.

Nombre del estudiante: Dario Fernando Cueva Granda

Código de estudiante: 00326896

C.I.: 2100691944

Lugar y fecha: Quito, 22 de diciembre de 2023

## **ACLARACIÓN PARA PUBLICACIÓN**

**Nota:** El presente trabajo, en su totalidad o cualquiera de sus partes, no debe ser considerado como una publicación, incluso a pesar de estar disponible sin restricciones a través de un repositorio institucional. Esta declaración se alinea con las prácticas y recomendaciones presentadas por el Committee on Publication Ethics COPE descritas por Barbour et al. (2017) Discussion document on best practice for issues around theses publishing, disponible en <http://bit.ly/COPETHeses>.

## **UNPUBLISHED DOCUMENT**

**Note:** The following graduation project is available through Universidad San Francisco de Quito USFQ institutional repository. Nonetheless, this project – in whole or in part – should not be considered a publication. This statement follows the recommendations presented by the Committee on Publication Ethics COPE described by Barbour et al. (2017) Discussion document on best practice for issues around theses publishing available on <http://bit.ly/COPETHeses>.

## DEDICATORIA

*A mamá y papá  
A mi hermana*

*To mom and dad  
To my big sis*

## AGRADECIMIENTOS

A la Universidad San Francisco de Quito por abrirme nuevamente sus puertas.

Al personal de Clydent S.A., particularmente a Daniel Aguilera por su colaboración en el presente proyecto y al personal técnico de sus laboratorios por la asistencia técnica durante la secuenciación de ADN.

A Alexis Debut y Karla Vizuete de la Universidad de las Fuerzas Armadas ESPE por su colaboración y paciencia en la obtención de las fotografías de microscopía electrónica de transmisión.

A Liseth Salinas y Lorena Mejía por su guía en los análisis de genómica comparativa, y a Bernardo Gutiérrez por su guía en los análisis filogenéticos.

A Gabriel Trueba y Lázaro López por su asesoría en los ensayos de susceptibilidad antimicrobiana.

A los miembros de mi comité de tesis, especialmente a Luís D. R. Melo por toda su asesoría en cuanto a la caracterización de los bacteriófagos.

A todos los miembros del grupo de biofilms del laboratorio de bacteriología en el Instituto de Microbiología por todo su apoyo a lo largo del presente proyecto. Especiales agradecimientos a Belén Atiencia Carrera por introducirme a las técnicas de caracterización de biofilms, a Nicolás Jara Medina, Karla Nolivos y Danilo Endara por su colaboración técnica en los ensayos experimentales.

A todos quienes me brindaron su amistad incondicional, especialmente a Danilo, Karla, Tamia, Dayana, Nicolás, Ariana, Génesis, Pamela, Belén, Carolina, María José, Santiago, Ronny, Bryan, María Paula Y.D.P., Andrea R., Andrea G., Aracely, Liseth S., Lizeth S., y Liseth S. A mis amigos me motivaron a la distancia, especialmente a Belén, I., Karen, N., Izan C., Paulita E., y Dario R.

A mi director de tesis por ser una excelente guía profesional y humana.

## RESUMEN

Las biopelículas representan una problemática en salud pública y la industria en debido a su incrementada resistencia a las terapias antimicrobianas. El uso de virus bacterianos (fagos), ha demostrado ser una alternativa prometedora para remover o evitar la formación de biopelículas, sin embargo, poco se conoce sobre las dinámicas de predación de los fagos en estas comunidades bacterianas a lo largo del tiempo. En el presente estudio se ha utilizado a *Vibrio* spp. y sus fagos como modelo de estudio de estas interacciones entre fagos y biopelículas. Se reporta la caracterización de 6 fagos virulentos con amplio espectro para *Vibrio* spp., 5 siphovirus del género *Mardecavirus*, y 1 podovirus correspondiente a un grupo no descrito anteriormente. Se probó el efecto individual o combinado (coctel) de bacteriófagos en biopelículas individuales y mixtas de *V. parahaemolyticus* y *V. alginoliticus*. Los resultados muestran de que los fagos fueron capaces de multiplicarse y reducir el número de bacterias susceptibles tanto en biopelículas individuales y mixtas en un corto tiempo (<8h), dañando la estructura de las biopelículas en el proceso. Sin embargo, las poblaciones bacterianas se recuperaron pese a las altas concentraciones de fagos en solución a medida que transcurrió el tiempo (48-72h). Los cocteles de fagos no mostraron tener un efecto superior en la reducción de células viables de las biopelículas mixtas en comparación a los fagos individuales, por el contrario, los recuentos bacterianos mostraron recuperarse más rápido en este caso. Sin embargo, la estructura de la película se vio mucho más afectada con cocteles que atacaban a las 2 bacterias. En conclusión, los fagos afectaron significativamente a las biopelículas, pero fueron incapaces de erradicarlas por completo. Se recomienda el uso de terapias combinadas para combatir a las bacterias restantes luego del tratamiento.

**Palabras clave:** Biopelículas, fagos, *Vibrio* especies, cocteles, erradicación.

## ABSTRACT

Biofilms are a problem in public health and industries due to their increased resistance to traditional antimicrobial therapy. The incumbent rise to pan-resistant bacteria increases the urge to find new approaches for biofilm control and eradication. Phage therapy has proved as a promising alternative to remove biofilms or inhibit their establishment. Yet, little is known about phage predation dynamics undergoing such protected microbial communities over time. In the present study, we have used *Vibrio* spp. and their phages as a model study for phage-biofilm interactions. We describe in detail six virulent phages with a wide-host range against *Vibrio* spp. Among them, we report five siphovirus *Mardecavirus* spp. candidates, and one novel podovirus. We challenged individual phages or cocktails against mono-species or mixed biofilms of *V. parahaemolyticus* and *V. alginolyticus*. We found that phages multiplied while reducing the number of viable susceptible bacteria both in single species and mixed biofilms within a short time span (<8h). Biofilm structure was compromised during this process. However, viable bacteria numbers were able to recover despite high phage titers over time (48-72h). Phage cocktails did not show a greater effect on viable cell reduction in mixed biofilms when compared to individual phages, and in fact, cell numbers recovered even faster when exposed to the cocktails. Yet, overall biofilm structure was more compromised with cocktails as the mixtures targeted both species at the same time. In conclusion, phages disrupted the biofilms but were unable to eradicate them. Further studies should explore combined treatments to eliminate the remaining bacteria after phages have acted on biofilms.

**Keywords:** Biofilm, phages, *Vibrio* species, cocktail, eradication.



## ÍNDICE DE CONTENIDOS

DEDICATORIA.....	5
AGRADECIMIENTOS.....	6
RESUMEN.....	7
ABSTRACT.....	8
ÍNDICE DE TABLAS.....	10
ÍNDICE DE FIGURAS.....	11
ÍNDICE DE ANEXOS.....	12
1. INTRODUCTION.....	13
2. MATERIALS AND METHODS.....	15
2.1. Reagents, equipment, and other resources.....	15
2.2. Bacterial isolation, growth conditions, and phenotypic characterization.....	15
2.3. Phage isolation.....	17
2.4. Phage selection, host range, and infection efficiency.....	19
2.5. Phage Transmission Electron Microscopy.....	21
2.6. Phage genome sequencing.....	22
2.7. Phage genome data analysis.....	23
2.8. Phage pH stability assay and quantitative data analysis.....	25
2.9. <i>Vibrio</i> -associated biofilm formation and initial characterization.....	25
2.10. Phage predation assays in single and dual-species <i>Vibrio</i> -associated biofilms.....	27
3. RESULTS.....	29
3.1. <i>Vibrio</i> and phage isolation, selection, and cross-interactions.....	29
3.2. Phage characterization.....	30
3.3. Preliminary characterization of dual-species <i>Vibrio</i> -associated biofilms.....	33
3.4. Phage dynamics in single-species biofilms.....	33
3.5. Phage cocktail dynamics in dual-species <i>Vibrio</i> biofilms.....	35
4. DISCUSSION.....	37
4.1. Phage infection characterization.....	37
4.2. Phage isolation and characterization.....	38
4.3. Phage effect on biofilms.....	39
5. CONCLUSIONS.....	42
REFERENCES.....	43
TABLES AND FIGURES.....	50

## ÍNDICE DE TABLAS

<b>Table 1:</b> Phage morphology and genome characteristics.....	50
--	----

## ÍNDICE DE FIGURAS

<b>Figure 1:</b> Phage infective, genomic, and stability characterization.....	51
<b>Figure 2:</b> Preliminary characterization of dual-species biofilm of <i>Vibrio</i> spp. over time.....	52
<b>Figure 3:</b> Effect of individual phages on single species biofilms of <i>V. alginolyticus</i> and <i>V. parahaemolyticus</i> .....	52
<b>Figure 4:</b> Effect of individual phages and phage cocktails on dual-species biofilms of <i>V. alginolyticus</i> and <i>V. parahaemolyticus</i> .....	53
<b>Figure 5:</b> Fluorescence microscopy images of biofilms of <i>V. alginolyticus</i> formed over coverslip glass and challenged against 3 individual phages.....	54
<b>Figure 6:</b> Fluorescence microscopy images of biofilms of <i>V. parahaemolyticus</i> formed over coverslip glass and challenged against 3 individual phages.....	55
<b>Figure 7:</b> Fluorescence microscopy images of mixed biofilms of <i>V. alginolyticus</i> and <i>V. parahaemolyticus</i> formed over coverslip glass and challenged against 3 individual phages and 2 phage cocktails.....	56

## ÍNDICE DE ANEXOS

<b>ANEXO A:</b> Antibiotic susceptibility test and biochemical results (Fig. S1).....	57
<b>ANEXO B:</b> Multiplex PCR for <i>Vibrio</i> species identification (Fig. S2).....	58
<b>ANEXO C:</b> Phage- <i>Vibrio</i> cross interactions from assay B (Fig. S3).....	59
<b>ANEXO D:</b> Phage- <i>Vibrio</i> cross interaction matrix reflecting multiplication efficiency of phages in different hosts (Fig. S4).....	60
<b>ANEXO E:</b> Transmission Electron Microscopy TEM microphotographs of ten isolated phages (Fig. S5).....	61
<b>ANEXO F:</b> Comparative genomic analysis of <i>Mardecavirus</i> phages (Fig. S6).....	62
<b>ANEXO G:</b> GC-skew analysis of the six sequenced phages in this study (Fig. S7).....	63
<b>ANEXO H:</b> Fluorescence microscopy reflecting individual light channels and merged images of 4 dual-species biofilms (Fig. S8).....	64
<b>ANEXO I:</b> Map of sampling sites (Fig. S9).....	65
<b>ANEXO J:</b> Summary of reagents, equipment, and resources mentioned in the Methods section (Supplementary Table 1).....	66
<b>ANEXO K:</b> Primer sequences used throughout the study (Supplementary Table 2)....	68
<b>ANEXO L:</b> Comparison of genome features and reported lifecycle of <i>Mardecavirus</i> spp. (Supplementary Table 3).....	69

## 1. Introduction

Marine microorganisms coexist in dynamic communities and are subject to competence, predation, and rapid environmental changes. Among them, *Vibrio* species are highly diverse and ubiquitous (Liang et al., 2019), and some species are known to cause infectious diseases in humans and/or aquaculture. For instance, the acute hepatopancreatic necrosis disease AHPND caused by *V. parahaemolyticus* results in up to 100% shrimp mortality in farms (Wang et al., 2015). This causes severe economic impacts as the shrimp industry has become one of the largest economic sections in many developing countries such as Ecuador.

Currently, the most adopted management practices against *Vibrio* include probiotics to improve water quality or compete directly with *Vibrio* spp. (Kumar et al., 2016), or the indiscriminate use of antibiotics to control outbreak events. Despite the efforts, *Vibrio* infections often persist in culture systems due to their biofilm-forming abilities. Biofilms are indeed the most prevalent form of bacterial communities in nature as this lifestyle facilitates gene exchange, provides shelter, and confers resistance to biotic and abiotic stressors. These protected communities are hard to eliminate from the surfaces they are attached to, and from here they constantly release microorganisms into the environment (Flemming et al., 2016; Sauer et al., 2022). Thus, new biofilm-released *Vibrio* might colonize or re-colonize water sources causing prolonged outbreaks (Teschler et al., 2015; Yildiz & Visick, 2009). Furthermore, the lack of appropriate water management in developing economies contributes to pathogen dissemination through water systems (Vinueza et al., 2021). Thus, finding effective ways to combat *Vibrio* by inhibiting biofilm formation, and, more importantly, disrupting mature biofilm structure is of extreme relevance to improve yields and reduce mortality in aquaculture farms.

One of the most promising approaches for biofilm control includes the use of phages (bacterial viruses) to either kill selectively pathogenic bacteria within biofilms or disrupt the architecture of the community (Pires et al., 2017; Salmond & Fineran, 2015). As obligate parasites, phages have perfected mechanisms to infect and kill their procaryotic host throughout evolution. This predatory dynamic has been studied to understand host-parasite interactions (Betts et al., 2018), coevolution (Hussain et al., 2021; Piel et al., 2022), and as a potential antimicrobial therapy (Gordillo Altamirano et al., 2022; Gordillo Altamirano & Barr, 2019). More recently, the study of *Vibrio* spp. and their specific phages has provided a great model to study phage-bacteria interactions in natural populations (Hussain et al., 2021; Kauffman et al., 2022; Piel et al., 2022), as well as the protective effect of multispecies biofilm architecture to phages (Winans et al., 2022).

So far, most studies that explore the effect of phages on biofilms in *Vibrio* spp. ( Kim et al., 2019) and elsewhere focus on analyzing an endpoint result rather than kinetic analysis over time (Abedon et al., 2021). Yet, in nature, bacteria form part of multispecies communities and are known to have a wide and changing array of defense genes that result in a susceptibility-resistance spectrum to phages (Hussain et al., 2021; Piel et al., 2022). Furthermore, the effect of one or multiple phages (known as cocktails) on biofilms has also been poorly explored and must be considered as a larger phage diversity might potentially accelerate bacterial resistance to phages (Betts et al., 2018). Thus, little is known about phage predation-dynamics within biofilms, particularly in those formed by multiple bacteria of different susceptibilities to phages.

Therefore, the present study aims to evaluate the application of phages against biofilm-forming *Vibrio* species and to understand phage-predation dynamics undergoing on single or multispecies biofilms. The present work characterized infection susceptibility of sixteen diverse wild-type *Vibrio* isolates from *V. parahaemolyticus*, *V. alginolyticus*, *V.*

*cholerae*, and *V. vulnificus* against sixteen wide-host range phages isolated from diverse Ecuadorian shrimp farms. Then, *V. parahaemolyticus* and *V. alginolyticus* isolates were applied to evaluate single and mixed biofilms and analyze the effect of individual phages or cocktails on such biofilms. Phage multiplication (PFU/mL), biofilm biomass (OD570), viable cell change (CFU/mL), and biofilm structure (LIVE/DEAD staining using fluorescence microscopy) were evaluated throughout the study.

## **2. Materials and Methods**

### **2.1. Reagents, equipment, and other resources**

Supplementary Table 1 presents a detailed list of resources (reagents, types of equipment, and software, among others) used and abbreviations described throughout the text.

### **2.2. Bacterial isolation, growth conditions, and phenotypic characterization**

Wildtype bacterial isolates were recovered from shrimp hatcheries, farms, packaging industries sewage, and seawater using CHROMagar<sup>TM</sup> Vibrio. Shrimp hatchery samples were collected either from larvae farms in the coast of Ecuador in the Province of Santa Elena, or the Gulph of Guayaquil once a transport ship arrived with fresh larvae to transfer to ponds. Samples from farms came from Taura in Durán, Puná Island on the Guayas River, or farms around the “Estero Salado” estuary, and corresponded to both large and small producers. Sewage samples came from packaging wastewater plants in Durán (Figure S9). The streak method was employed for the isolation of distinct colored colonies according to the manufacturer’s instructions. Plates were incubated at 30 °C for 24 hours. Individual colonies were passed and grown at 30 °C for 24 hours in TSA supplemented with NaCl to reach a final concentration of 1.5% w/v and in TCBS to register their ability to break down sucrose for further presumptive *Vibrio parahaemolyticus* identification.

Individual isolates were preserved in 2 mL vials containing TSB supplemented with 20% w/v glycerol in a -80 °C freezer for long-term storage. Three hundred and twenty-one bacterial isolates were recovered from a hundred samples over six months. Thirty isolates from different presumptive species were chosen randomly from diverse sampling locations for phenotypical characterization assays. The API 20E tests for gram-negative bacteria were conducted according to the manufacturer's instructions using a solution of 1.5% NaCl for bacterial suspensions as it has been shown to improve upon *Vibrio* spp. identification accuracy based on differential substrates used (Martinez-Urtaza et al., 2006). Further phenotypic characterization of each isolate was performed through an antibiotic susceptibility profile obtained according to the CLSI M45 3<sup>rd</sup> ed. Guide for *Vibrio* spp. The antibiotics from the following families were tested: penicillins (AM, AMC), cepheims (CTX, CAZ, FEP), fluoroquinolones (CIP), carbapenems (IPM), Folate Pathway inhibitors (SXT), aminoglycosides (GM), phenicols ©, and tetracyclines (TE, D). The diffusion disk test was performed as specified in the guide using MHA for all the antibiotics but TE. Here the minimal inhibitory concentration test was performed accordingly in MHB.

Bacterial species confirmation was performed through multiplex PCR. Bacterial DNA was extracted through the boiling method (Salinas et al., 2020). Briefly, a few colonies of a fresh pure culture were picked with a sterile toothpick and suspended in 200 µL AE buffer (Tris-HCl pH9 10mM, EDTA 0.5 mM) in 1.5 mL Eppendorf tubes. Tubes were suspended in a boiling water bath for 10 minutes and then immediately cooled in an ice bath for 15 minutes. Samples were centrifuged at 13000 rpm for 10 minutes, and supernatants were transferred to a new Eppendorf tube. DNA was quantified in a NanoDrop One and diluted if necessary. PCR reactions were carried out under the following conditions: a volume of 15µL, 0.5 units of GoTaq Flexi DNA polymerase, 1X



GoTaq Green PCR buffer, 1.5 mM MgCl<sub>2</sub>, 0.2μM of each primer for *Vibrio* spp. (Supplementary Table 2) 0.2 mM of dNTPs mix, and 5 ng of DNA. The temperature profile included an initial denaturation of 3 minutes, 30 cycles of denaturation at 95 °C for 10 seconds, and a combined annealing/extension step at 65 °C for 30 seconds, followed by a final extension at 72 °C for 5 min. Fragments were determined using 2% w/v agarose gel electrophoresis with SYBR Safe staining using a 100 bp fragment standard. Gels were run at 80V for 1 hour and revealed in a molecular imager. At least three PCR assays were performed on different days.

Fourteen out of the thirty characterized isolates were chosen for further assays based on their different origin, phenotypic profiles, and species confirmation. Two more *Vibrio* sp. isolates from contaminated seafood in local markets and kept at the microbial collection of the Institute of Microbiology of Universidad San Francisco de Quito (IM-USFQ) were used in our assays to increase the diversity of wild-type isolates. These isolates were previously identified using 16s RNA gene sequencing and used as positive controls for our PCR analysis. In total, our final bacterial panel was comprised of six *Vibrio parahaemolyticus* wildtype isolates (from now on abbreviated as VP), four *V. alginolyticus* (VA) isolates, five *V. cholerae* (VC) isolates, and one *V. vulnificus* (VV) isolate.

### **2.3. Phage isolation**

Bacteriophage isolation was conducted from the diverse water samples previously mentioned. Two assays were set for phage enrichment targeting: A) *V. parahaemolyticus*, and B) *Vibrio* spp. To obtain phages for VP (Assay A), we first established a bank of presumptive VP bacteria isolated allopatrically, based on their CHROMagar distinctive mauve color development and their lack of ability to break down sucrose on TCBS agar.

Since we obtained many bacterial isolates, we performed the enrichment pooling up to 5 isolates as further described. Water samples were enriched using a sterile 10x concentrated peptone and yeast extract broth (peptone 100 g/L, yeast extract 50 g/L, K<sub>2</sub>HPO<sub>4</sub> 80 g/L). 100mL mixtures were prepared in 250mL sterile glass flasks using 90 mL of sample water and 10 mL of 10x broth. Bacterial inoculum to provide host bait for phage multiplication consisted of 200 µL of an exponential culture in TSB (supplemented with NaCl to reach a concentration of 1.5%) of each isolate. Assays were incubated at room temperature for 48 hours with no agitation. Afterward, ten milliliters of the enriched samples were put into 15 mL falcon tubes and centrifuged at 6000 rpm for 10 minutes. Supernatants were passed through a 0.20 µm syringe filter and stored in sterile 10 mL capped test tubes at 4 °C until the phages' presence could be determined. To obtain phages for any *Vibrio* sp. isolates (Assay B), we used all the isolated bacteria from a given water sample as inoculum for host bait using the enriched water from the same source (sympatrically). Around one hundred water samples were enriched, evaluating for phages from Assay B. In this case, water samples were stored for up to a week at 4 °C before the inoculum could be performed, as bacterial hosts required subcultures before they could be used. The rest of the procedure was performed as previously described.

We used a spot test to assess the presence of phages in the enriched filtrates (Melo et al., 2014). Briefly, 4 mL of a molten soft overlay agar (TSB 15 g/L, NaCl 12.5 g/L, Bacto agar 7 g/L) at 50 °C were vortex mixed (at 500 rpm) with 1 mL of bacterial culture (at OD<sub>600</sub> of 0.5) and quickly poured into a solid TSA NaCl 1.5% media. Petri dishes were allowed to rest for about 5 minutes to allow overlay agar jelling, and then 2 µL drops of each filtered sample were carefully added on top of the overlay. Drops were allowed to dry for a few minutes before incubation for 24 hours at 30°C. A sample was deemed positive for containing phages if spots, where bacterial growth did not occur, were

present. Drops from multiple samples were tested simultaneously in a petri dish with a presumptive host. Samples that did not have lytic activity in any host were discarded. At least two spot test assays were performed on different days.

Samples with lytic activity against a bacterial host were ten-fold serially diluted in PBS, and a 2  $\mu$ L spot test of the serial dilutions was carried out to test for the presence of reproductive phages. If individual plaques were observed, a double-layer spread plate assay was performed with that given sample. Briefly, 4 mL of molten soft overlay agar were mixed (at 500 rpm) with 1 mL of an exponential bacterial culture (OD<sub>600</sub> 0.5) of the specific bacterial host and 100  $\mu$ L of the phage dilution that displayed the lowest count of individual phage plaques in the spot test. Mixes were poured into TSA-NaCl 1.5% media. Samples were incubated for 24 hours at 30 °C. Individual plaques were picked with a sterile 1 mL pipette tip and suspended in 15 mL sterile falcon tubes containing 10 mL TSB NaCl 1.5% inoculated with 200  $\mu$ L of an exponential culture of the respective host. The tubes were incubated for 24 hours at 30 °C, and the following day the tubes were centrifuged for 10 minutes at 6000 rpm. Supernatants were recovered and 10-fold serially diluted to repeat the double-layer spread plate technique. This process was performed at least five more times to obtain individual phages. The final supernatants were passed through a 0.20  $\mu$ m syringe filter and stored at 4 °C.

#### **2.4. Phage selection, host range, and infection efficiency**

Fifty-seven isolated phages from assay A were spot-tested against forty VP isolates. A matrix of host range for phages isolated for *V. parahaemolyticus* was constructed (2280 cross-interactions, data not shown). Nine phages (Pvp7, Pvp9, Pvp21, Pvp31, Pvp38, Pvp42, Pvp48, Pvp52, and Pvp73), isolated allopatrically with the diverse 40 *V. parahaemolyticus* hosts with the broadest (but substantially different) host range in VP

isolates were selected for further assays. A hundred phage-positive solutions from assay B, isolated sympatrically with their *Vibrio* sp. host, were spot-tested in our diverse sixteen-bacteria panel (Figure S3) comprised of four species (resulting in 1600 cross-interactions). Here, we selected seven additional good candidates (Pva1-Pva7), and some of them displayed a multispecies-host range which has been rarely described for *Vibrio* species infecting oysters (Piel et al., 2022). We named eight phages recovered from assay A with the code Pvp since VP was their primary target, while seven phages obtained from assay B were named with the code Pva since VA was their most prominent target. A phage isolated from assay A (Pvp73) was later identified as a phage for *V. alginolyticus* due to its more efficient multiplication in VA hosts and so it was later named Pva73. Thus, we ended up with 8 Pvp and 8 Pva phages. The sixteen phages were titter counted in each of the bacteria that they were able to infect from the panel of sixteen bacteria to evaluate their infection efficiency in multiple hosts (a.k.a efficiency of plating, EOP). First, solutions of a titter of  $1 \times 10^9$  plaque-forming units (PFU)/mL of each phage were prepared. Then, ten-fold serial dilutions ( $1 \times 10^0 - 1 \times 10^8$ ) of phage solutions were performed in PBS, and 10  $\mu$ L of each serial dilution was spotted into an overlay agar with their respective host. If a phage could produce lysis in the first or second dilution of the spot test but could not produce individual phage plaques in more diluted samples we classified the interaction as lysis without phage production (Delbrück, 1940; Hussain et al., 2021; Piel et al., 2022). This procedure was performed in triplicate and the number of plaques present in the 10  $\mu$ L drop in a countable dilution were used to estimate phage titters and estimate the EOP in each host. Finally, ten phage candidates (Pvp21, Pvp31, Pvp38, Pvp42, Pvp52, Pva73, Pva1, Pva3, Pva4, and Pva7) based on their ability to infect different hosts were selected for transmission electron microscopy (TEM) analysis.

## **2.5. Phage Transmission Electron Microscopy**

TEM microphotographs were obtained using concentrated phage solutions ( $>1.0 \times 10^{12}$  PFU/mL) in water (Ackermann, 2009). Confluent phage lysis in a double-layer agar culture was used as a starter. Shortly, twenty microliters of stored 4 °C phage stocks were spread in about two-thirds of a petri dish with TSA-NaCl 1.5% using a sterile swab. Then 1 mL of an exponential culture of the bacterial host was inoculated in molten soft overlay agar at 50 °C, mixed (at 500 rpm), and immediately poured on top of the phage-containing agar plate. Plates were allowed to solidify and incubated for 24 hours at 30 °C (Jakočiūnė & Moodley, 2018). The next day, the top soft agar layer was removed and placed in a 15 mL falcon tube. Four milliliters of autoclaved distilled water were added, and the tubes were thoroughly vortexed (at 3000 rpm) for one minute and then incubated at 4 °C for 24 hours. Vortex (at 3000 rpm) was applied for one minute afterward, and then the tubes were centrifuged for 15 minutes at 6000 rpm. Supernatants were recovered using a 10 mL syringe, and samples were passed through a 0.20 µm filter and full into two 1.5 mL Eppendorf conical tubes. Phages were concentrated using a refrigerated centrifuge at 4 °C and 21,000 *g* for 4 hours. Most of the supernatant was carefully removed without disturbing the pellet, and 200 µL of autoclaved distilled water were added (Ackermann, 2009). The tubes were thoroughly mixed (at 3000 rpm) until no pellet was left. This wash procedure was repeated twice. Ten microliters of the phage solutions were used to perform a quick phage titer estimation as previously described, and at this point, the average phage count after the procedure was about  $5.0 \times 10^{12}$  PFU/mL.

Ten microliters of phage solutions were stained for 10 seconds with phosphotungstic acid (PTA) 1%, then quickly transferred into a copper grid. Microphotographs were obtained at 80kV using an FEI-Tecnai G20 Spirit Twin microscope equipped with an Eagle 4k HR camera. Image J/Fiji software v1.53k (Collins, 2007; Schindelin et al., 2012) was used to

perform measurements of the head diameter (Hd), head length (Hl), tail diameter (Td), and tail length (Tl). At least five individual virions were measured in each sample (Melo et al., 2014), and the values correspond to the measurements' average. Phage family determination was performed according to the morphology and dimensions of the virions (Ackermann, 2009).

## **2.6. Phage genome sequencing**

Phage DNA extraction was performed according to Jakočiūnė and Moodley's protocol (Jakočiūnė & Moodley, 2018) with several modifications to improve DNA concentration. 180  $\mu\text{L}$  of concentrate phage solutions ( $>1.0 \times 10^{12}$  PFU/mL) were put into 1.5 mL Eppendorf tubes and 20  $\mu\text{L}$  of 10X RQ1 DNase reaction buffer (400mM Tris-HCl pH 8.0, 100 mM  $\text{MgSO}_4$  and 10 mM  $\text{CaCl}_2$ ) was added. Tubes were mixed and 2  $\mu\text{L}$  of RQ1 DNase (1 u/ $\mu\text{L}$ ) were added and mixed. 2  $\mu\text{L}$  of RNase A solution (4 mg/mL) were added. Samples were incubated at 37 °C for two hours. The high-sensitivity dsDNA detection kit was used to evaluate complete extra-capsid DNA digestion using a Qubit fluorometer. Then, 20  $\mu\text{L}$  of DNase stop solution (EDTA 0.5 M, pH 8) were added, and samples were incubated in a heating block at 65 °C for 15 minutes. Samples were cooled to reach room temperature. The DNeasy blood and tissue kit was used to perform the nucleic acid extractions. 5  $\mu\text{L}$  of proteinase K were added to the tubes and samples were incubated at 56°C for 2 hours. 250  $\mu\text{L}$  of buffer AL was added and vortex mixed (at 1500 rpm) followed by incubation at 70 °C for 10 minutes. 250  $\mu\text{L}$  of absolute ethanol were mixed (at 1500 rpm) into the tube, and the resulting 750  $\mu\text{L}$  were loaded into the spin column. Columns were centrifuged for 1 minute at 6,000 g and transferred into a new collection tube. 500  $\mu\text{L}$  of AW1 solution was added, and columns were centrifuged for 1 minute at 6,000 g. Columns were transferred into new collection tubes, and 500  $\mu\text{L}$  of

AW2 solution was added. Columns were centrifuged for 3 minutes at 20,000 g. Finally, columns were placed into 1.5 mL Eppendorf tubes, and 50 µL of AE buffer were added and centrifuged for 1 minute at 6,000 g (Jakočiūnė & Moodley, 2018). The 50 µL were passed two more times through the column to improve extraction yield. DNA was quantified using a Qubit fluorometer and a nanodrop spectrophotometer to measure concentration and quality. 1% agarose gel electrophoresis with SyberSafe staining was used to evaluate DNA integrity.

Six phages were selected through their morphologies from the initial ten phages evaluated by TEM analysis (see Table 1), more exactly five siphovirus and one podovirus were sequenced using long sequence read technology using an ONT minION. The genomic library was prepared using the ligation sequencing DNA kit (SQK-LSK14) following the manufacturer's instructions. Each phage was sequenced individually, and the base call was performed using the High Accuracy base-calling (HAC) model (Kelly et al., 2023). Due to the size of the genomes being small and each of them being separate, the achieved sequencing depth was 200,000 x.

### ***2.7. Phage genome data analysis***

First, a nucleotide blast was performed using the NCBI blast search tool (<https://blast.ncbi.nlm.nih.gov/Blast.cgi>) with the whole genome sequences of the phages. In our case, the five sequenced siphovirus belonged to the same genus, thus we performed comparative and phylogenetic analysis between them and with similar available genomes on the NCBI nucleotide database.

Genome annotations were performed using Bakta (Schwengers et al., 2021), BV-BRC-PATRIC (Olson et al., 2023), UniProt protein BLAST (Pundir et al., 2017), and visualized using SnapGene Viewer v7.0.2 and Proksee (Grant et al., 2023). Additionally, antibiotic-

resistance genes were searched within the genomes using RESFINDER (Florensa et al., 2022). The large terminase subunit was identified in the annotations and defined as the starting point for comparative analysis as has been done previously for vibriophages (Piel et al., 2022). EasyFig v2.1 (Sullivan et al., 2011) was used to display pairwise comparisons and homology levels between the annotated genomes. Meanwhile, the progressiveMauve (Darling et al., 2010) was used to identify genome rearrangements and gene gains or losses of our phages compared among them and with sequences available in the NCBI nucleotide database (<https://www.ncbi.nlm.nih.gov/nucleotide/>).

Genome alignment was carried out with the Cyclic DNA Sequence Aligner CSA (Fernandes et al., 2009) to rotate the circular permuted genomes and set the same starting point, while the whole genome alignment was performed using MAFFT v7 (Kato & Standley, 2013) afterward. Phylogenetic analyses were made with BEAST 2.7.4 (Bouckaert et al., 2014). Twenty million Markov-Chain Monte Carlo iterations were performed under the GTR+I+G substitution model (Lanave et al., 1984). This nucleotide substitution model was selected according to Bayesian Information Criterion BIC scores (Neath & Cavanaugh, 2012) in MEGA X (Kumar et al., 2018). A tip-calibrated tree was obtained under the Coalescent Constant Population Model using the sampling year for each sample as tip dates. Tree annotator was used to generate the Maximum Clade Credibility MCC tree, using a 20% burn-in. The consensus MCC tree was generated using FigTree v1.4.4 displaying posterior probability values for each node and divergence times between different clades. Finally, a comparison of the phage's main structural proteins, namely the major capsid protein (MCP) and the major tail tube (MTP) protein, was performed with the amino acid sequence obtained from Snap Gene Viewer v7.0.2. Amino acid sequence alignments were performed to identify substitutions and variants of the



proteins were modeled using Phyre2 (Kelley et al., 2015) using intensive settings and Swiss-Model servers (Waterhouse et al., 2018).

### **2.8. Phage pH stability assay and quantitative data analysis**

For pH stability tests, 10  $\mu\text{L}$  of concentrated phage suspensions ( $1 \times 10^{11}$  PFU/mL) were used to inoculate 1 mL of appropriated buffered solutions (acetate buffer 0.1 M for low pH, PBS for neutral pH, and Tris 0.1M at high pH). The pH values were adjusted to 2.0, 4.0, 7.0, 9.0, and 11.0 with 1 M NaOH or 1 M HCl. The tubes were then incubated at 25  $^{\circ}\text{C}$  and aliquots were taken after 60 min for phage quantification using 10-fold dilutions on soft TSA-NaCl 1.5% as previously described (Kim et al., 2019). Four independent assays were performed and the differences in phage counts at each pH were analyzed using a Kruskal-Wallis non-parametric test, followed by Dunn's test using the Bonferroni correction for the multiple comparisons within groups at  $\alpha = 0.05$  using “*ggstatsplot*” v0.12.1 package (Patil, 2021). Boxplots of the phage counts were plotted using “*ggplot2*” v3.4.3 package (Wickham, 2016) in R software (Ihaka & Gentleman, 1996).

### **2.9. Vibrio-associated biofilm formation and initial characterization**

In a previous study, the impact of the initial inoculum and temperature on *V. parahaemolyticus* and *V. cholerae*. biofilm's cell viability, biomass, cell mortality, and biofilm structure over time (Jara-Medina et al., *in-review*). Here, we chose 4 bacterial combinations consisting of two different isolates of VA, VP, and VC from our 16-bacteria panel based on the phage's ability to differentially infect and multiply in the bacteria (see Figure S4). Dual species biofilms were formed on TSB NaCl 1.5% as previously used for Vibrio-associated biofilm formation (Kim et al., 2019) with a total inoculum of  $1 \times 10^7$  colony-forming units (CFU)/mL ( $0.5 \times 10^7$  CFU/mL for each isolate). Biofilms 1 and 2

consisted of a mix of VP and VA isolates, while biofilms 3 and 4 were composed of a mix of VC and VA isolates. More specifically, biofilm B1 was formed by VP87 and VA235, biofilm B2 was constituted by VP125 and VA170, biofilm B3 was elaborated by VA62 and VC94, and finally biofilm B4 was composed by VA62 and VC112. Sterile cell-culture-treated 6-well plates were used for biofilm establishment on sterile glass coverslips (submerged in 96% ethanol and flamed). In brief, 3 mL of inoculated broth was placed on each well and incubated without agitation at 30 °C. Biofilms were allowed to form over 24 h and 72 h to compare cell viability counts, and biofilm structure differences in newly formed and established biofilms.

After incubation, excess broth and planktonic cells were removed from biofilms. Coverslips on well plates were washed twice using sterile PBS, and then mounted on glass slides for fluorescence microscopy or placed on a falcon tube with 10 mL of PBS for bacterial counts. A Live/Dead biofilm viability kit was used to observe bacterial communities. Two hundred milliliters of a solution of propidium iodide (PI, at 0.01 mM) and SYTO-9 (at 0.06 mM) were used to stain the coverslips for 20 minutes at room temperature under dark conditions. Slides were visualized under an x100 immersion objective using the appropriate light filters for the fluorescent dyes. Ten random microscopic fields were imaged from each slide. A composite image from the 2 color channels was obtained using ImageJ v1.53k. Falcon tubes were vortex mixed, and ten-fold serial dilutions per performed. A hundred microliters of dilutions  $10^{-4}$  and  $10^{-5}$  were spread-plated on CHROMagar Vibrio™ using the spread plate technique. Incubation conditions were set as previously described. Four independent assays were performed in duplicate and differences in viable cell counts were analyzed using a Kruskal-Wallis non-parametric and Dunn's test using as previously described for phage-pH assays.

## **2.10. Phage predation assays in single and dual-species *Vibrio*-associated biofilms**

Single and dual-species biofilms of VP125 and VA170 were formed on 24-well plates for measurement with different quantitative methods and 6-well culture plates for biofilm structure observation.

For 24-well plates, one milliliter of a solution TSB-NaCl 1.5% containing bacteria in concentrations of  $1 \times 10^7$  CFU/mL (for single-species biofilms  $1 \times 10^7$  CFU/mL, for dual-species biofilms  $0.5 \times 10^7$  CFU/mL of each for a total count of  $1 \times 10^7$ ) in each well. Wells containing TSB-NaCl 1.5% media without inoculum were placed as sterility control.

Plates were placed in a shaking incubator at 25 °C and 120 rpm. Each 24 h over 72 h, the media in the wells was carefully removed, and the bottom was washed once with PBS to remove the excess free cells without disturbing the bottom and replaced with one milliliter of fresh broth, as realized in previous studies (Atiencia-Carrera et al., 2022; Cabezas-Mera et al., 2023).

At the end of the biofilm formation, supernatants (media plus planktonic cells) were carefully removed, and biofilms were washed twice with sterile PBS. For single-species biofilms, the phages Pvp21, Pva73, and Pva1 at MOI 1, and a control treatment without phage were used as described in other studies to test the effect of phages on biofilms (Melo et al., 2020). This corresponded to a phage treatment of  $1 \times 10^8$  PFU/mL, similar phage titers applied previously to characterize the phage effect of *V. alginolyticus* biofilms (S. G. Kim et al., 2019). In this case, the phage Pva1 was able to infect and multiply in both bacteria, and the other phages were specific in their ability being able to multiply in their host (Pvp21 multiplied in VP but not VA, while Pva73 multiplied in VA but not VP). For dual-species biofilm, the same three phages were used individually to observe their effect and specificity in each of the bacterium hosts, and two phage cocktails

(more exactly, Phage Mix 1 containing Pvp21, Pva73, and Pva1, and Phage Mix 2 containing Phage Mix 1 plus Pvp52, Pva3, and Pva7) were used to evaluate if a greater phage diversity had a different effect on biofilm eradication assays, as previously it has been observed that bacteria might evolve defense mechanisms in different ways when challenged with a higher diversity of phages in *in-vitro* planktonic assays (Betts et al., 2018). In the case of the phage cocktails, equal amounts of each phage were applied, and the total applied cocktail contained  $1 \times 10^8$  PFU/mL of the phage mix. A negative control with no phage was also used. Plates were incubated at 25 °C and 120 rpm. Phages were applied only at the beginning of the treatment and no medium change was performed. Biofilms and the phage effect on them were monitored at times 0, 4, 8, 24, and 48 h being time zero as the time when new broth with or without phage treatment (negative control) was added. For each sampling point, phages were tittered from supernatants while for biofilms present on the bottom of wells viable cell counts, bacteria mortality in the remaining biofilm, and biomass measurements were performed. In brief, one milliliter of supernatant broth was placed in a conical 1.5 mL microtube and then centrifuged at 17,000 g for 5 minutes. Clear supernatants were serially diluted 1:10 and plated in their specific hosts by the number of PFU on soft TSA-NaCl 1.5% (Kim et al., 2019). Pvp21 was plated on VP125, Pva73, and Pva1 on VA170, while Phage Mix 1 and Phage Mix 2 were plated both on VP125 and VA170 to evaluate the total number of phages able to infect each of the bacteria. To obtain bacterial counts, Biofilms were washed twice with PBS, and then one milliliter of PBS was added. Biofilms were scraped and thoroughly mixed using a sterile pipette tip. An aliquot of two hundred microliters for each biofilm was put into a 96-well plate and a Tecan plate reader was used to measure absorbance at 570nm as a gross measurement of biofilm biomass. Sterile PBS was used as blank. Another one-hundred microliter aliquot was put in a glass slide and dyed with a cell

viability kit to perform estimations of bacterial mortality within the remaining biofilm as previously described. Serial 10-fold dilutions were performed from the remaining bacterial suspensions and cell counts of bacteria were performed on CHROMagar™ Vibrio medium using the microdrop counting method described in other studies (Melo et al., 2020; Pires et al., 2017) to be able to differentiate viable cells from each species in mixed biofilms. We also used this culture media to count single-species biofilms as the isolate VA170 was able to produce swarming making it unable to distinguish single colonies on other culture media different than CHROMagar™ Vibrio.

Single and dual-species biofilms were also formed on 6-well plates with a coverslip glass. Treatment and concentrations were applied identically to biofilms formed on 24-well plates. In every sampling point, biofilms were washed, coverslips were carefully removed, placed on a glass slide, and dyed for Live/Dead biofilm viability evaluation as previously described. Ten random microscopic fields were imaged from each slide. A composite image from the 2 color channels was obtained using ImageJ v1.53k (Collins, 2007).

### **3. Results**

#### **3.1. *Vibrio and phage isolation, selection, and cross-interactions***

Three hundred and twenty-one *Vibrio* sp. Isolates were recovered during the sampling of this study from shrimp hatcheries, farms, and wastewater of shrimp packaging plants. Fifty-seven phages were isolated with presumptive *V. parahaemolyticus* of allopatric origin as host bait. In addition, a hundred phage-enriched cultures were obtained using any recovered *Vibrio* spp. of sympatric origin. The 57 *V. parahaemolyticus* phages (from now on referred to as Pvp phages) were challenged against 40 *V. parahaemolyticus*

isolates corresponding to 3380 cross-interactions (data not shown). Eight Pvp phages with the widest host range or with differences in host ranges were selected for further assays. A few (30) bacteria out of the 321 isolated *Vibrio* spp. were selected based on the diversity of type of water source and geographical location, and their different presumptive species identification using CHROMagar Vibrio™. Sixteen of these bacterial isolates were confirmed as *V. parahaemolyticus*, *V. cholerae*, *V. alginolyticus*, or *V. vulnificus* with further biochemical tests (Figure S1) and multiplex PCR (Figure S2). Antibiotic resistance was found in the majority of these isolates. Fifteen bacteria were resistant or intermediate resistant to one or more than one of the twelve antibiotics from eight antibiotic classes tested, and one bacterium showed sensitivity to all antibiotics (Figure S1). These diverse bacteria were used to isolate phages with a different or multi-species host range from the 100 phage-containing solutions. This corresponded to 1600 additional cross-interactions (Figure S3). Eight additional phages capable of replication in isolates of *V. alginolyticus* or both *V. alginolyticus* and *V. parahaemolyticus* were selected (from now on referred to as Pva phages). Out of the sixteen Pvp and Pva phages, eight candidates showed a multispecies range when challenged against the sixteen chosen bacteria (Figure S4). Finally, the simplified diverse cross-interaction panel suggested that phage replication occurs modular manner (Figure S4).

### **3.2. Phage characterization**

From the initial set, ten phages were selected for further characterization. After transmission electron microscopy (TEM) analysis, nine of them showed a siphovirus morphology, while one phage was a podovirus (Figure S5). Due to the siphovirus's similar morphological size (Table 1) and host range (Figure 1a and Figure S4), only five siphovirus and the podovirus were selected for genome characterization.

All the siphovirus candidates belonged to the *Mardecavirus* genus. Comparative analysis showed that these five siphoviruses maintain synteny, with a high conservation level across most genes (Figure 1c). The most variable parts of the genomes belonged to the tail fibers protein gene, a few tail assembly protein genes, an uncharacterized protein gene among structure-related genes, and a region that contained hypothetical proteins. An extremely high homology was found in the main structural proteins, major capsid protein (MCP), and major tail protein (MTP). Further translation analysis (data not shown) revealed that the amino acids sequence is 100% identical among the different phages (except by only 1 amino-acid substitution in 1 of the five phages). We did not find any lysogeny-associated or transduction-associated genes, such as replicative integrase or transposase in concordance with previous studies that have analyzed hundreds of Vibriophages (Hussain et al., 2021; Piel et al., 2022). Antibiotic-resistance genes, or tRNAs were not identified within the phage genomes. Some recombination proteins such as *recA* and *ruvC*, or endonucleases from a large family of nuclease-associated proteins called “HNH proteins” (Figure 1c) were identified.

Further comparisons of our group set with the genomes available in the GenBank suggested that some phages have the ability to gain some DNA segments (Figure S6). No inversions or segment translocations were detected, yet a duplicated segment that contained hypothetical protein genes in one phage (Pva73) was found.

Phylogenetic analysis showed that our five siphovirus come from two distinct clades (Figure 1b). Specifically, phages whose replication was the most efficient in the *V. parahaemolyticus* isolates (such as Pvp21 and Pvp52) were differentiated from the phages whose replication was the most efficient in *V. alginolyticus* (Pva1, Pva3, and Pva73; Figures 1a and 1b). When comparing Pva1 and Pva3 genomes, they seem to be very closely related (Figure 1b), yet Pva1 had also acquired the ability to replicate in both *V.*

*alginolyticus* and *V. parahaemolyticus*, although the efficiency with which it multiplies in the latter host was a thousand-fold lower (see Figure 1a).

Finally, genomic analysis of the podovirus candidate showed that it is very likely a new type of phage. Only a very small fragment of the genome (17%, see Table 1) had a moderate similarity (74.74%, Table 1) to a recently discovered podovirus for *V. alginolyticus* known as the Vibrio phage vB\_ValP\_VA-RY-3 (Ren et al., 2022). Most of the genome annotations consisted of hypothetical proteins (Figure 1c), and only five non-structural genes were identified, namely an ATP-dependent RNA helicase, an Exonuclease, DNA ligase, Thymidylate synthase, and a DNA polymerase. No structural proteins could be identified based on DNA or amino acid homology. The GC skew analysis of this phage showed that its genome possesses an odd configuration as half of the genome is rich in GC and the open reading frames (ORFs) are predicted in one DNA strand, while the other half of the genome has a low GC content and the ORFs are in the other DNA strand (Figure S7).

Regarding their stability in different pH conditions, we did not find any differences in phage titers at neutral pH, and only two of them (more exactly, Pvp21 and Pva73) were significantly affected when exposed to acidic conditions of pH 4 (Figure 1d). The phage Pvp52 remained stable from very acidic conditions of pH 2 to alkaline conditions of pH 11, losing only 1 10-log fold of titers in extreme conditions. On the contrary, the phage Pva73 resulted in the most affected at lower pH, while the phage Pva3 viability reduced significantly at higher pH values. Thus, we observe in these closely related phages a difference in their tolerance to different environmental conditions.



### **3.3. Preliminary characterization of dual-species *Vibrio*-associated biofilms**

We selected seven *Vibrio* sp. isolates (more exactly, VP87, VP125, VA170, VA235, VA62, VC94, and VC112) based on their different degrees of susceptibility and permissibility to phage infection (Figure 1a and Figure S4) and paired them in groups of two to evaluate if they were able to establish stable biofilms over time. In total, four dual-species biofilms consisting of different bacteria combinations were tested. More exactly, these paired groups were denominated B1 (VP87 and VA235), B2 (VP125 and VA170), B3 (VA62 and VC94), and B4 (VA62 and VC112), as shown in Figure 2. No differences in the viable cell populations in biofilms formed using any combination of *V. parahaemolyticus* and *V. alginolyticus* were observed, but the biofilms containing *V. alginolyticus* and *V. cholerae* experienced a reduction of viable cell numbers up to a hundred less viable *V. cholerae* in the mixed biofilm over time (Figure 2a). Additionally, we observed that at 72 hours, the biofilms had more complex structures than at 24 hours showing signs of a more mature state (Figure 2b and Figure S8). Ultimately, the 72 h biofilms formed by *V. parahaemolyticus* 125 the *V. alginolyticus* 170 were selected to evaluate the effect of different phages and their mix combinations due to the higher resistance to external pressures reported on mature biofilms (Cangui-Panchi et al., 2022, 2023; Flemming et al., 2016).

### **3.4. Phage dynamics in single-species biofilms**

Three phages were selected based on their capacity to infect either the selected isolate of *V. parahaemolyticus*, *V. alginolyticus*, or both. More exactly, the phage Pvp21 targeting *V. parahaemolyticus*, Pva73 targeting *V. alginolyticus*, and Pva1 targeting both *Vibrio* species were chosen. However, it is important to mention that Pva1 phage demonstrated much less efficiency in *V. parahaemolyticus* when compared to *V. alginolyticus*. Our

results evidenced that the phages were able to affect the bacteria in biofilms in a very specific manner (Figure 3). For example, Pvp21 showed a significant reduction of cell viability and biofilm biomass exclusively on *V. parahaemolyticus*, more exactly a 2 log fold reduction in cell numbers within 8 hours of phage exposure, without affecting *V. alginolyticus* even though the phage can cause bacteria lysis when in very high concentrations (Figure 3a). Thus, it is possible to observe that the infection is not sufficient for the phage to eradicate the biofilm, but the permissibility of the bacteria and the chain-effect of new virions play an important role in the biofilm disruption. Likewise, Pva73 and Pva1 also demonstrated a significant effect on both cell viability and biomass of *V. alginolyticus* (Figures 3a and 3b). Although Pva1 showed more than a thousand times less efficiency in multiplying into *V. parahaemolyticus*, there was a significant effect on both cell viability and biomass on this host from 24h forward (Figures 3a and 3b).

When exploring the phage treatment in a longitudinal analysis, all phages with an efficient replication (i.e. Pva1 vs VA or Pvp21 vs VP) demonstrated a significant effect in a short period (peaking at eight hours). However, biofilms were able to recover after phage treatments, more exactly after forty-eight hours. This is particularly evident when analyzing the effect on cell viability of both phages targeting *V. alginolyticus* (Fig 3a).

In summary, all phages were capable of significantly disrupting the biofilms, but unable to eradicate them. Both Pva73 and Pva1 phages of *V. alginolyticus* were able to reduce cell viability around a thousand times (more exactly, 3 log reduction at its peak), while Pvp21 was able to reduce cell viability of the *V. parahaemolyticus* biofilm by approximately a hundred times (or 2 log reduction at its peak). Meanwhile, cell counts on the control biofilms without phage or in the biofilms not targeted by the specific phages (such as VA vs Pvp21) showed no effect in cell counts when compared to the results

obtained with functional phages such as VA vs Pva73. Overall results suggested that the efficiency of phage treatment directly depends on the response of the bacteria (i.e., the initial resistance to phages or the appearance of resistant bacteria sooner or later). These results concord with the changes we observed in the biofilm structure over time. For instance, in the case of *V. alginolyticus* (Figure 5), we found a disruption of biofilm structure within the first eight hours when challenged with the specific phages Pva1 and Pva73. No major effect when the non-specific phage Pvp21 was applied. On the other hand, the opposite is true for changes in biofilm structure in *V. parahaemolyticus* (Figure 6). There was no apparent effect within the first eight hours with either of the Pva phages, but differences were observed when the Pvp21 phage was applied. Interestingly, the phage Pva1 shows an effect by 24 hours, which matches the results of this phage effect on cell viability (CFU/mL, Figure 3) that revealed a delayed effect of this phage on the biofilms.

Phage titers varied accordingly, for instance, we observed a quick rise (by 4h) of titers when challenging phages to susceptible bacteria (i.e. Pvp21 vs VP, or Pva73 vs VA), and a slow rise of phage (by 48h) numbers when considering the phage and bacteria interaction that displays a reduced phage multiplication efficiency (Pva1 vs VP). Finally, as expected, no differences were found in phage titers when exposing non-susceptible bacteria to them.

### **3.5. Phage cocktail dynamics in dual-species *Vibrio* biofilms**

After the characterization of the individual effect of the selected phages on single-species biofilms, all individual phages plus two phage cocktails were further analyzed on dual-species multi-species *Vibrio* biofilms (Figure 4), more exactly a cocktail containing the three phages and a more diverse phage cocktail containing three additional phages for a

total of six phages. This evaluation aimed to characterize if individual phages were still able to partially disrupt the dual-species biofilm or if a protective effect from the non-targeted bacteria occurred, as well as if a more diverse set of phages was able to have a better or worse effect on biofilm eradication.

First, we observed a significant increase in phage titers in all treatments, either in individual phages or cocktails. Our results showed that the individual phages were able to specifically interact with the target *Vibrio* species within the dual biofilms and reduce their cell viability (Figure 4a), but with no effect of the non-target *Vibrio* sp. Surprisingly, cocktails were less effective in reducing biofilm viability than individual phages. For instance, Pvp21 showed a significant effect when acting alone on *V. parahaemolyticus*, but there was no significant effect on this bacterial species when the phage was in a mix with two other phages targeting the other bacteria (Cocktail 1: Pvp21, Pva73, and Pva1) or acting together with another phage (Pvp52) also targeting *V. parahaemolyticus* and four other phages targeting *V. alginolyticus* (Cocktail 2: Pvp21, Pvp52, Pva73, Pva1, Pva3, and Pva7). In the case of *V. alginolyticus*, individual phages also showed a significant effect when acting alone (Pva73 or Pva1), but this effect was less prominent in both cocktails regardless of containing two or four specific phages (Figure 4a). So, there is to discussion about why the cocktails with phages targeting both bacteria were not able to reduce the viability of them both.

Interestingly, we found that the phage with impaired infection (Pvp21 vs VA) that did not influence biofilms formed exclusively by *V. alginolyticus*, was able to reduce the viable cell numbers of this bacteria by 72h, potentially due to the high titers of this phage produced over time when multiplying in *V. parahaemolyticus* (Figure 4a). On the other hand, contrary to what we observed in single-species biofilms of *V. parahaemolyticus*, we did not observe a significant effect by the phage with a less efficient multiplication

(Pva1 vs VP). So, we observe how bacteria that are not the main phage target might be impacted differently by phages produced by other bacteria in the community.

When analyzing the effect of phages on biofilm biomass, we observe that a few of them are capable of reducing the biomass within the first 4 hours of the application (Figure 4b), more exactly, Pvp21, Cocktail 1, and Cocktail2. Furthermore, only Cocktail 1 containing three phages, and the phages Pva1, Pva73, and Pvp21 targeting both bacteria demonstrated higher biomass reduction when compared to the other phages, or combination of phages. Finally, regarding biofilm structure, we confirmed with fluorescence microscopy that biofilm structure was disrupted with the application of both individual phages or cocktails (Figure 7). However, cocktails seem to have a better effect on biofilm structure disruption as they target both species within the biofilm.

## **4. Discussion**

### ***4.1. Phage infection characterization***

The present study demonstrated that our phages replicated in their hosts in a species-modular manner as previously described for *Vibrio* spp. (Kauffman et al., 2022). Some phages were not able to multiply in the bacteria they infected, particularly in *V. cholerae* (Figure 1a and Figure S4). This result has been described for *Vibrio* spp. as impaired infection (Piel et al., 2022) or lysis from without (Hussain et al., 2021). Likewise, certain phages often would multiply with different efficiencies in those hosts that were permissive for virion production. Both impaired or limited phage replication have been attributed to the bacterial innate defense mechanisms, while non-entry is attributed to structural differences in phage-bacteria interaction proteins (Hussain et al., 2021; Piel et al., 2022).

#### **4.2. Phage isolation and characterization**

Our five newly characterized siphovirus are members of *Mardecavirus* spp. This group contains phages that are exclusive to *Vibrio* spp. (Alanis Villa et al., 2012; Brossard Stoos et al., 2022; Kim et al., 2021; Lee et al., 2012; Li et al., 2023; Srisangthong et al., 2023; Wong et al., 2019; Xia et al., 2022; Yu et al., 2018). Initially, phages from this genus were classified as temperate or transducing phages (Supplementary table 3) (Alanis Villa et al., 2012; Lee et al., 2012), mainly due to having recombinases within their genomes that might participate in recombination with host genomes. Lately, phages from this genus have been classified as lytic (Li et al., 2023; Srisangthong et al., 2023; Xia et al., 2022). Recently, several studies have pointed out that the role of recombinase genes in marine viruses is probably to exchange genes among them rather than integration or recombination with bacteria (Hussain et al., 2021; Kauffman et al., 2022; Piel et al., 2022). So, it is plausible that the extra segments we found in certain phages originated from the exchange of genetic information with other coexisting phages via recombination rather than obtaining these segments from the bacterial hosts. When analyzing the GC-skew of these phages, we found random fluctuations in the content of GC from 30.5% to 57.5% at most (Figure S7), so it seems unlikely that segments from external sources with a different GC content are present in the phage genomes. For comparison, *V. parahaemolyticus* has a slightly lower GC content (45.5%) (Klein et al., 2018) than our *Mardecavirus* spp. phages (48.8%, see Table 1). When conducting a guided search for the homology of these phages with *Vibrio* spp., we did not find matches to any accession provided little to no evidence of DNA trace of *Mardacavirus* phages in *Vibrio* genomes. As such, phages were considered adequate for biofilm assays as no evidence of integration was found.

We were not able to perform any genomic comparative analysis with our podovirus candidate as little homology was found with known phages, or any DNA sequence for that matter. No structural proteins were identified, thus further phylogenetic comparisons with the widely used MCP or MTP be performed to address the relationship of this virus with other podovirus. Thus, we potentially propose this phage to be a new *genus* candidate.

Spite the two approaches to isolate phages (sympatrically and allopatrically), nine out of the ten initial phages of interest resulted in a similar siphovirus morphology. After sequencing, we confirmed that indeed the siphovirus were very closely related. This suggests a bias of isolation as phages from a very specific group were recovered. We recommend using alternative phage recovery methods such as flocculation rather than enrichment to obtain a greater diversity of phages as has been done previously for *Vibrio* spp (Hussain et al., 2021; Piel et al., 2022).

#### ***4.3. Phage effect on biofilms***

We observed that phages interacted with bacteria in the biofilms in a very specific manner, depending on the bacteria susceptibility, and virion chain-effect over time.

First, in single-species biofilms, we found, that biofilms formed by fully susceptible bacteria to phages were affected in a short time, with a rapid phage titer increase. On the other hand, biofilms challenged with phages with a reduced multiplication efficiency were also affected, although the effect was less significant and appeared after longer exposure to phages. Accordingly, phage titers showed a slow increase in numbers and only after a prolonged time of exposure. Biofilms formed by non-susceptible bacteria were, as expected, not affected by phages. These differences are attributed to bacterial defense mechanisms which could potentially impact the number of phages produced in

each round of infection (Hussain et al., 2021; Piel et al., 2022), and how quickly the infective chain-effect caused by new virions occurs. Currently, we do not know the burst size of the phages in each of the hosts, thus further analyses are necessary to confirm the relationship existing between phage infective latency and burst size, and the effect on the biofilms. In *Vibrio* spp. phage resistance is attributed to variability in the accessory genome of the bacteria. Specifically, the presence of innate defense mechanisms such as restriction enzymes, or abortive infective systems provides bacteria with defenses against phages even at the clonality level (Hussain et al., 2021). The number and redundancy of defense mechanisms result in a spectrum of resistance to phages that goes from a reduced multiplication efficiency to a completely impaired infection (Piel et al., 2022). Through this fashion, bacteria can quickly adapt to phage predation while the core genome can remain stable for normal functioning and communication where mutation of receptors targeted by phages would possibly involve a reduced fitness due to an impact on physiological functions (i.e. quorum sensing signaling, biofilm formation, etc.) (Hussain et al., 2021). Further genomic analyses on our bacterial hosts are recommended to help unravel the defense mechanisms involved in the resistant phenotypes we observed and that are important to consider when targeting bacteria with phages.

When analyzing mixed biofilms, we observed that individual phages affected only susceptible bacteria where phages could multiply efficiently, but the populations of these bacteria were able to recover as observed in single-species biofilms. Our results showed that the effect of phage cocktails was less significant on individual bacteria compared to the treatments where individual phages were used. This could be attributed to two reasons, first each phage was diluted in relationship to the whole phage cocktail as the cocktails were formed by mixing equal parts of each phage to maintain an overall concentration of  $1 \times 10^8$ . In the case of cocktail 1, each phage was present in a third of the concentration



when compared to individual treatment. In cocktail 2, each phage had 1/6 of the initial concentration. Thus, variations in initial concentrations of individual phages might have affected the chain-effect caused by virions produced during the initial infection cycles, as the MOI can have an impact on how bacteria react to phages and recover over time (S. G. Kim et al., 2019). Further analysis of how phage concentration impacts biofilms would be worth exploring to design the best treatment possible for further industrial applications. Second, it has been recently observed that increases in the diversity of phages infecting a host accelerate its adaptation and diversification. Thus, bacteria coevolve at the genome level from a fluctuating (Red Queen hypothesis) to a directional evolutionary (arms race hypothesis) (Betts et al., 2018). So, it is also possible that the increased phage diversity in the cocktails might have accelerated the resistance we observed in the first place. Finally, it is also possible that resistance to phages could have been transferred from one bacterium to the other, as phage defense elements in *Vibrio* spp. have been found to rapidly disseminate through mobile genetic elements (Hussain et al., 2021), and as biofilms provide a perfect niche for genetic exchange (Flemming et al., 2016). More research is necessary to determine if the reduced effect of cocktails on cell viability is attributed to one or more reasons mentioned above. Finally, we recommend exploring combined therapies to eliminate the remaining bacteria after phages have acted on biofilms as synergy has been observed when combined phages with traditional therapy (Akturk et al., 2019).

## 5. CONCLUSIONS

The present study isolated six virulent phages and tested them individually and in different combinations against single or multispecies *Vibrio* spp. biofilms. It was demonstrated that these phages were able to disrupt susceptible bacterial communities in mature biofilms within a short time span. Overall results suggested that phage effectiveness depends on bacterial susceptibility. In addition, the selected cocktails did not show a greater effect than individual phages when targeting mixed communities. In all cases, biofilms recovered bacterial viability over time despite high phage titers. Thus, further studies should evaluate the combination of different treatments to successfully eradicate single and multi-species *Vibrio*-related biofilms.

## REFERENCES

- Abedon, S. T., Danis-Wlodarczyk, K. M., Wozniak, D. J., & Sullivan, M. B. (2021). Improving Phage-Biofilm In Vitro Experimentation. *Viruses*, *13*(6), 1175. <https://doi.org/10.3390/v13061175>
- Ackermann, H.-W. (2009). Basic Phage Electron Microscopy. In M. R. J. Clokie & A. M. Kropinski (Eds.), *Bacteriophages* (Vol. 501, pp. 113–126). Humana Press. [https://doi.org/10.1007/978-1-60327-164-6\\_12](https://doi.org/10.1007/978-1-60327-164-6_12)
- Akturk, E., Oliveira, H., Santos, S. B., Costa, S., Kuyumcu, S., Melo, L. D. R., & Azeredo, J. (2019). Synergistic Action of Phage and Antibiotics: Parameters to Enhance the Killing Efficacy Against Mono and Dual-Species Biofilms. *Antibiotics*, *8*(3), 103. <https://doi.org/10.3390/antibiotics8030103>
- Alanis Villa, A., Kropinski, A. M., Abbasifar, R., Abbasifar, A., & Griffiths, M. W. (2012). Genome Sequence of Temperate *Vibrio parahaemolyticus* Bacteriophage vB\_VpaS\_MAR10. *Journal of Virology*, *86*(24), 13851–13852. <https://doi.org/10.1128/JVI.02666-12>
- Atiencia-Carrera, M. B., Cabezas-Mera, F. S., Vizuete, K., Debut, A., Tejera, E., & Machado, A. (2022). Evaluation of the biofilm life cycle between *Candida albicans* and *Candida tropicalis*. *Frontiers in Cellular and Infection Microbiology*, *12*, 953168. <https://doi.org/10.3389/fcimb.2022.953168>
- Betts, A., Gray, C., Zelek, M., MacLean, R. C., & King, K. C. (2018). High parasite diversity accelerates host adaptation and diversification. *Science*, *360*(6391), 907–911. <https://doi.org/10.1126/science.aam9974>
- Bouckaert, R., Heled, J., Kühnert, D., Vaughan, T., Wu, C.-H., Xie, D., Suchard, M. A., Rambaut, A., & Drummond, A. J. (2014). BEAST 2: A Software Platform for Bayesian Evolutionary Analysis. *PLoS Computational Biology*, *10*(4), e1003537. <https://doi.org/10.1371/journal.pcbi.1003537>
- Brossard Stoos, K. A., Ren, J., Shields-Cutler, R. R., Sams, K. L., Caldwell, S., Ho, M. B., Rivara, G., Whistler, C. A., Jones, S. H., Wiedmann, M., DeMent, J., Getchell, R. G., & Marquis, H. (2022). Coastal water bacteriophages infect various sets of *Vibrio parahaemolyticus* sequence types. *Frontiers in Microbiology*, *13*, 1041942. <https://doi.org/10.3389/fmicb.2022.1041942>
- Cabezas-Mera, F. S., Atiencia-Carrera, M. B., Villacrés-Granda, I., Proaño, A. A., Debut, A., Vizuete, K., Herrero-Bayo, L., Gonzalez-Paramás, A. M., Giampieri, F., Abreu-Naranjo, R., Tejera, E., Álvarez-Suarez, J. M., & Machado, A. (2023). Evaluation of the polyphenolic profile of native Ecuadorian stingless bee honeys (Tribe: Meliponini) and their antibiofilm activity on susceptible and multidrug-resistant pathogens: An exploratory analysis. *Current Research in Food Science*, *7*, 100543. <https://doi.org/10.1016/j.crfs.2023.100543>
- Cangui-Panchi, S. P., Ñacato-Toapanta, A. L., Enríquez-Martínez, L. J., Reyes, J., Garzon-Chavez, D., & Machado, A. (2022). Biofilm-forming microorganisms causing hospital-acquired infections from intravenous catheter: A systematic

- review. *Current Research in Microbial Sciences*, 3, 100175. <https://doi.org/10.1016/j.crmicr.2022.100175>
- Cangui-Panchi, S. P., Ñacato-Toapanta, A. L., Enríquez-Martínez, L. J., Salinas-Delgado, G. A., Reyes, J., Garzon-Chavez, D., & Machado, A. (2023). Battle royale: Immune response on biofilms – host-pathogen interactions. *Current Research in Immunology*, 4, 100057. <https://doi.org/10.1016/j.crimmu.2023.100057>
- Carpenter, A. E., Jones, T. R., Lamprecht, M. R., Clarke, C., Kang, I., Friman, O., Guertin, D. A., Chang, J., Lindquist, R. A., Moffat, J., Golland, P., & Sabatini, D. M. (2006). CellProfiler: Image analysis software for identifying and quantifying cell phenotypes. *Genome Biology*, 7(10), R100. <https://doi.org/10.1186/gb-2006-7-10-r100>
- Collins, T. J. (2007). ImageJ for microscopy. *BioTechniques*, 43(1S), S25–S30. <https://doi.org/10.2144/000112517>
- Darling, A. E., Mau, B., & Perna, N. T. (2010). progressiveMauve: Multiple Genome Alignment with Gene Gain, Loss and Rearrangement. *PLoS ONE*, 5(6), e11147. <https://doi.org/10.1371/journal.pone.0011147>
- Delbrück, M. (1940). The growth of bacteriophage and lysis of the host. *The Journal of General Physiology*, 23, 643–660.
- Fernandes, F., Pereira, L., & Freitas, A. T. (2009). CSA: An efficient algorithm to improve circular DNA multiple alignment. *BMC Bioinformatics*, 10(1), 230. <https://doi.org/10.1186/1471-2105-10-230>
- Flemming, H.-C., Wingender, J., Szewzyk, U., Steinberg, P., Rice, S. A., & Kjelleberg, S. (2016). Biofilms: An emergent form of bacterial life. *Nature Reviews Microbiology*, 14(9), 563–575. <https://doi.org/10.1038/nrmicro.2016.94>
- Florensa, A. F., Kaas, R. S., Clausen, P. T. L. C., Aytan-Aktug, D., & Aarestrup, F. M. (2022). ResFinder – an open online resource for identification of antimicrobial resistance genes in next-generation sequencing data and prediction of phenotypes from genotypes. *Microbial Genomics*, 8(1). <https://doi.org/10.1099/mgen.0.000748>
- Gordillo Altamirano, F. L., & Barr, J. J. (2019). Phage Therapy in the Postantibiotic Era. *Clinical Microbiology Reviews*, 32(2), e00066-18. <https://doi.org/10.1128/CMR.00066-18>
- Gordillo Altamirano, F. L., Kostoulas, X., Subedi, D., Korneev, D., Peleg, A. Y., & Barr, J. J. (2022). Phage-antibiotic combination is a superior treatment against *Acinetobacter baumannii* in a preclinical study. *eBioMedicine*, 80, 104045. <https://doi.org/10.1016/j.ebiom.2022.104045>
- Grant, J. R., Enns, E., Marinier, E., Mandal, A., Herman, E. K., Chen, C., Graham, M., Van Domselaar, G., & Stothard, P. (2023). Proksee: In-depth characterization and visualization of bacterial genomes. *Nucleic Acids Research*, 51(W1), W484–W492. <https://doi.org/10.1093/nar/gkad326>
- Hussain, F. A., Dubert, J., Elsherbini, J., Murphy, M., VanInsberghe, D., Arevalo, P., Kauffman, K., Rodino-Janeiro, B. K., Gavin, H., Gomez, A., Lopatina, A., Le Roux, F., & Polz, M. F. (2021). Rapid evolutionary turnover of mobile genetic

- elements drives bacterial resistance to phages. *Science*, 374(6566), 488–492. <https://doi.org/10.1126/science.abb1083>
- Ihaka, R., & Gentleman, R. (1996). R: A Language for Data Analysis and Graphics. *Journal of Computational and Graphical Statistics*, 5(3), 299–314. <https://doi.org/10.1080/10618600.1996.10474713>
- Jakočiūnė, D., & Moodley, A. (2018). A Rapid Bacteriophage DNA Extraction Method. *Methods and Protocols*, 1(3), 27. <https://doi.org/10.3390/mps1030027>
- Katoh, K., & Standley, D. M. (2013). MAFFT Multiple Sequence Alignment Software Version 7: Improvements in Performance and Usability. *Molecular Biology and Evolution*, 30(4), 772–780. <https://doi.org/10.1093/molbev/mst010>
- Kauffman, K. M., Chang, W. K., Brown, J. M., Hussain, F. A., Yang, J., Polz, M. F., & Kelly, L. (2022). Resolving the structure of phage–bacteria interactions in the context of natural diversity. *Nature Communications*, 13(1), 372. <https://doi.org/10.1038/s41467-021-27583-z>
- Kelley, L. A., Mezulis, S., Yates, C. M., Wass, M. N., & Sternberg, M. J. E. (2015). The Phyre2 web portal for protein modeling, prediction and analysis. *Nature Protocols*, 10(6), 845–858. <https://doi.org/10.1038/nprot.2015.053>
- Kelly, A., Went, S. C., Mariano, G., Shaw, L. P., Picton, D. M., Duffner, S. J., Coates, I., Herdman-Grant, R., Gordeeva, J., Drobiazko, A., Isaev, A., Lee, Y.-J., Luyten, Y., Morgan, R. D., Weigele, P., Severinov, K., Wenner, N., Hinton, J. C. D., & Blower, T. R. (2023). Diverse Durham collection phages demonstrate complex BREX defense responses. *Applied and Environmental Microbiology*, 89(9), e00623-23. <https://doi.org/10.1128/aem.00623-23>
- Kim, H.-J., Kim, Y.-T., Kim, H. B., Choi, S. H., & Lee, J.-H. (2021). Characterization of bacteriophage VVP001 and its application for the inhibition of *Vibrio vulnificus* causing seafood-borne diseases. *Food Microbiology*, 94, 103630. <https://doi.org/10.1016/j.fm.2020.103630>
- Kim, H.-J., Ryu, J.-O., Lee, S.-Y., Kim, E.-S., & Kim, H.-Y. (2015). Multiplex PCR for detection of the *Vibrio* genus and five pathogenic *Vibrio* species with primer sets designed using comparative genomics. *BMC Microbiology*, 15(1), 239. <https://doi.org/10.1186/s12866-015-0577-3>
- Kim, S. G., Jun, J. W., Giri, S. S., Yun, S., Kim, H. J., Kim, S. W., Kang, J. W., Han, S. J., Jeong, D., & Park, S. C. (2019). Isolation and characterisation of pVa-21, a giant bacteriophage with anti-biofilm potential against *Vibrio alginolyticus*. *Scientific Reports*, 9(1), 6284. <https://doi.org/10.1038/s41598-019-42681-1>
- Klein, S., Pipes, S., & Lovell, C. R. (2018). Occurrence and significance of pathogenicity and fitness islands in environmental vibrios. *AMB Express*, 8(1), 177. <https://doi.org/10.1186/s13568-018-0704-2>
- Kumar, S., Stecher, G., Li, M., Knyaz, C., & Tamura, K. (2018). MEGA X: Molecular Evolutionary Genetics Analysis across Computing Platforms. *Molecular Biology and Evolution*, 35(6), 1547–1549. <https://doi.org/10.1093/molbev/msy096>
- Kumar, V., Roy, S., Meena, D. K., & Sarkar, U. K. (2016). Application of Probiotics in Shrimp Aquaculture: Importance, Mechanisms of Action, and Methods of

- Administration. *Reviews in Fisheries Science & Aquaculture*, 24(4), 342–368. <https://doi.org/10.1080/23308249.2016.1193841>
- Lanave, C., Preparata, G., Sacone, C., & Serio, G. (1984). A new method for calculating evolutionary substitution rates. *Journal of Molecular Evolution*, 20(1), 86–93. <https://doi.org/10.1007/BF02101990>
- Lee, H. S., Choi, S., & Choi, S. H. (2012). Complete Genome Sequence of *Vibrio vulnificus* Bacteriophage SSP002. *Journal of Virology*, 86(14), 7711–7711. <https://doi.org/10.1128/JVI.00972-12>
- Li, Z., Ren, Y., Wang, Z., Qi, Z., Murtaza, B., & Ren, H. (2023). Characterization and genomic analysis of the vibrio phage R01 lytic to *Vibrio parahaemolyticus*. *Aquaculture Reports*, 30, 101628. <https://doi.org/10.1016/j.aqrep.2023.101628>
- Liang, J., Liu, J., Wang, X., Lin, H., Liu, J., Zhou, S., Sun, H., & Zhang, X.-H. (2019). Spatiotemporal Dynamics of Free-Living and Particle-Associated *Vibrio* Communities in the Northern Chinese Marginal Seas. *Applied and Environmental Microbiology*, 85(9), e00217-19. <https://doi.org/10.1128/AEM.00217-19>
- Martinez-Urtaza, J., Lozano-Leon, A., ViÑ±a-Feas, A., Novoa, J., & Garcia-Martin, O. (2006). Differences in the API 20E biochemical patterns of clinical and environmental *Vibrio parahaemolyticus* isolates. *FEMS Microbiology Letters*, 255(1), 75–81. <https://doi.org/10.1111/j.1574-6968.2005.00052.x>
- Melo, L. D. R., Pinto, G., Oliveira, F., Vilas-Boas, D., Almeida, C., Sillankorva, S., Cerca, N., & Azeredo, J. (2020). The Protective Effect of *Staphylococcus epidermidis* Biofilm Matrix against Phage Predation. *Viruses*, 12(10), 1076. <https://doi.org/10.3390/v12101076>
- Melo, L. D. R., Sillankorva, S., Ackermann, H.-W., Kropinski, A. M., Azeredo, J., & Cerca, N. (2014). Isolation and characterization of a new *Staphylococcus epidermidis* broad-spectrum bacteriophage. *Journal of General Virology*, 95(2), 506–515. <https://doi.org/10.1099/vir.0.060590-0>
- Neath, A. A., & Cavanaugh, J. E. (2012). The Bayesian information criterion: Background, derivation, and applications. *WIREs Computational Statistics*, 4(2), 199–203. <https://doi.org/10.1002/wics.199>
- Neogi, S. B., Chowdhury, N., Asakura, M., Hinenoya, A., Haldar, S., Saidi, S. M., Kogure, K., Lara, R. J., & Yamasaki, S. (2010). A highly sensitive and specific multiplex PCR assay for simultaneous detection of *Vibrio cholerae*, *Vibrio parahaemolyticus* and *Vibrio vulnificus*: Detection of pathogenic *Vibrio* species. *Letters in Applied Microbiology*, 51(3), 293–300. <https://doi.org/10.1111/j.1472-765X.2010.02895.x>
- Olson, R. D., Assaf, R., Brettin, T., Conrad, N., Cucinell, C., Davis, J. J., Dempsey, D. M., Dickerman, A., Dietrich, E. M., Kenyon, R. W., Kuscuoglu, M., Lefkowitz, E. J., Lu, J., Machi, D., Macken, C., Mao, C., Niewiadomska, A., Nguyen, M., Olsen, G. J., ... Stevens, R. L. (2023). Introducing the Bacterial and Viral Bioinformatics Resource Center (BV-BRC): A resource combining PATRIC, IRD and ViPR. *Nucleic Acids Research*, 51(D1), D678–D689. <https://doi.org/10.1093/nar/gkac1003>

- Patil, I. (2021). Visualizations with statistical details: The “ggstatsplot” approach. *Journal of Open Source Software*, 6(61), 3167. <https://doi.org/10.21105/joss.03167>
- Piel, D., Bruto, M., Labreuche, Y., Blanquart, F., Goudenège, D., Barcia-Cruz, R., Chenivresse, S., Le Panse, S., James, A., Dubert, J., Petton, B., Lieberman, E., Wegner, K. M., Hussain, F. A., Kauffman, K. M., Polz, M. F., Bikard, D., Gandon, S., Rocha, E. P. C., & Le Roux, F. (2022). Phage–host coevolution in natural populations. *Nature Microbiology*, 7(7), 1075–1086. <https://doi.org/10.1038/s41564-022-01157-1>
- Pires, D., Melo, L., Vilas Boas, D., Sillankorva, S., & Azeredo, J. (2017). Phage therapy as an alternative or complementary strategy to prevent and control biofilm-related infections. *Current Opinion in Microbiology*, 39, 48–56. <https://doi.org/10.1016/j.mib.2017.09.004>
- Pires, D. P., Dötsch, A., Anderson, E. M., Hao, Y., Khursigara, C. M., Lam, J. S., Sillankorva, S., & Azeredo, J. (2017). A Genotypic Analysis of Five *P. aeruginosa* Strains after Biofilm Infection by Phages Targeting Different Cell Surface Receptors. *Frontiers in Microbiology*, 8, 1229. <https://doi.org/10.3389/fmicb.2017.01229>
- Pundir, S., Martin, M. J., & O’Donovan, C. (2017). UniProt Protein Knowledgebase. In C. H. Wu, C. N. Arighi, & K. E. Ross (Eds.), *Protein Bioinformatics* (Vol. 1558, pp. 41–55). Springer New York. [https://doi.org/10.1007/978-1-4939-6783-4\\_2](https://doi.org/10.1007/978-1-4939-6783-4_2)
- Ren, Y., Wang, L., Chen, R., Li, X., Li, S., Li, J., Li, Q., Wang, Z., & Xu, Y. (2022). Isolation and characterization of a novel phage vB\_ValP\_VA-RY-3 infecting *Vibrio alginolyticus*. *Virus Research*, 322, 198945. <https://doi.org/10.1016/j.virusres.2022.198945>
- Salinas, A. M., Osorio, V. G., Pacha-Herrera, D., Vivanco, J. S., Trueba, A. F., & Machado, A. (2020). Vaginal microbiota evaluation and prevalence of key pathogens in ecuadorian women: An epidemiologic analysis. *Scientific Reports*, 10(1), 18358. <https://doi.org/10.1038/s41598-020-74655-z>
- Salmond, G. P. C., & Fineran, P. C. (2015). A century of the phage: Past, present and future. *Nature Reviews Microbiology*, 13(12), 777–786. <https://doi.org/10.1038/nrmicro3564>
- Sauer, K., Stoodley, P., Goeres, D. M., Hall-Stoodley, L., Burmølle, M., Stewart, P. S., & Bjarnsholt, T. (2022). The biofilm life cycle: Expanding the conceptual model of biofilm formation. *Nature Reviews Microbiology*, 20(10), 608–620. <https://doi.org/10.1038/s41579-022-00767-0>
- Schindelin, J., Arganda-Carreras, I., Frise, E., Kaynig, V., Longair, M., Pietzsch, T., Preibisch, S., Rueden, C., Saalfeld, S., Schmid, B., Tinevez, J.-Y., White, D. J., Hartenstein, V., Eliceiri, K., Tomancak, P., & Cardona, A. (2012). Fiji: An open-source platform for biological-image analysis. *Nature Methods*, 9(7), 676–682. <https://doi.org/10.1038/nmeth.2019>
- Schwengers, O., Jelonek, L., Dieckmann, M. A., Beyvers, S., Blom, J., & Goesmann, A. (2021). Bakta: Rapid and standardized annotation of bacterial genomes via alignment-free sequence identification. *Microbial Genomics*, 7(11). <https://doi.org/10.1099/mgen.0.000685>

- Srisangthong, I., Sangseedum, C., Chaichanit, N., Surachat, K., Suanyuk, N., & Mittraparp-arthorn, P. (2023). Characterization and Genome Analysis of *Vibrio campbellii* Lytic Bacteriophage OPA17. *Microbiology Spectrum*, *11*(2), e01623-22. <https://doi.org/10.1128/spectrum.01623-22>
- Sullivan, M. J., Petty, N. K., & Beatson, S. A. (2011). Easyfig: A genome comparison visualizer. *Bioinformatics*, *27*(7), 1009–1010. <https://doi.org/10.1093/bioinformatics/btr039>
- Teschler, J. K., Zamorano-Sánchez, D., Utada, A. S., Warner, C. J. A., Wong, G. C. L., Linington, R. G., & Yildiz, F. H. (2015). Living in the matrix: Assembly and control of *Vibrio cholerae* biofilms. *Nature Reviews Microbiology*, *13*(5), 255–268. <https://doi.org/10.1038/nrmicro3433>
- Vinueza, D., Ochoa-Herrera, V., Maurice, L., Tamayo, E., Mejía, L., Tejera, E., & Machado, A. (2021). Determining the microbial and chemical contamination in Ecuador's main rivers. *Scientific Reports*, *11*(1), 17640. <https://doi.org/10.1038/s41598-021-96926-z>
- Wang, R., Zhong, Y., Gu, X., Yuan, J., Saeed, A. F., & Wang, S. (2015). The pathogenesis, detection, and prevention of *Vibrio parahaemolyticus*. *Frontiers in Microbiology*, *6*. <https://doi.org/10.3389/fmicb.2015.00144>
- Waterhouse, A., Bertoni, M., Bienert, S., Studer, G., Tauriello, G., Gumienny, R., Heer, F. T., de Beer, T. A. P., Rempfer, C., Bordoli, L., Lepore, R., & Schwede, T. (2018). SWISS-MODEL: Homology modelling of protein structures and complexes. *Nucleic Acids Research*, *46*(W1), W296–W303. <https://doi.org/10.1093/nar/gky427>
- Wei, S., Zhao, H., Xian, Y., Hussain, M. A., & Wu, X. (2014). Multiplex PCR assays for the detection of *Vibrio alginolyticus*, *Vibrio parahaemolyticus*, *Vibrio vulnificus*, and *Vibrio cholerae* with an internal amplification control. *Diagnostic Microbiology and Infectious Disease*, *79*(2), 115–118. <https://doi.org/10.1016/j.diagmicrobio.2014.03.012>
- Wickham, H. (2016). *Ggplot2*. Springer International Publishing. <https://doi.org/10.1007/978-3-319-24277-4>
- Winans, J. B., Wucher, B. R., & Nadell, C. D. (2022). Multispecies biofilm architecture determines bacterial exposure to phages. *PLOS Biology*, *20*(12), e3001913. <https://doi.org/10.1371/journal.pbio.3001913>
- Wong, H., Wang, T.-Y., Yang, C.-W., Tang, C.-T., Ying, C., Wang, C.-H., & Chang, W.-H. (2019). Characterization of a lytic vibriophage VP06 of *Vibrio parahaemolyticus*. *Research in Microbiology*, *170*(1), 13–23. <https://doi.org/10.1016/j.resmic.2018.07.003>
- Xia, H., Yang, H., Yan, N., Hou, W., Wang, H., Wang, X., Wang, H., & Zhou, M. (2022). Bacteriostatic effects of phage F23s1 and its endolysin on *Vibrio parahaemolyticus*. *Journal of Basic Microbiology*, *62*(8), 963–974. <https://doi.org/10.1002/jobm.202200056>
- Yildiz, F. H., & Visick, K. L. (2009). *Vibrio* biofilms: So much the same yet so different. *Trends in Microbiology*, *17*(3), 109–118. <https://doi.org/10.1016/j.tim.2008.12.004>



Yu, J., Lim, J.-A., Kwak, S.-J., Park, J.-H., & Chang, H.-J. (2018). Comparative genomic analysis of novel bacteriophages infecting *Vibrio parahaemolyticus* isolated from western and southern coastal areas of Korea. *Archives of Virology*, *163*(5), 1337–1343. <https://doi.org/10.1007/s00705-018-3756-3>

## TABLES AND FIGURES

**Table 1:** Phage morphology and genome characteristics.

Phage	Morphology (hl, hd, tl, td)	Genome (bp)	%GC	ORF	tRNA	Closest relative	Identity %	Query Cover %	Taxonomy ID
Pvp21	Siphovirus (94, 57, 132, 7)	Linear 76 668	48.8	107	-	<a href="#">Vibrio phage SSP002</a>	98.08	95	<i>Mardecavirus</i> spp.
Pvp52	Siphovirus (97, 59, 157, 9)	Linear 76 789	48.8	103	-	<a href="#">Vibrio phage SSP002</a>	97.99	97	<i>Mardecavirus</i> spp.
Pva73	Siphovirus (104, 62, 151, 7)	Linear 80 983	48.4	109	-	<a href="#">Vibrio phage VVP001</a>	97.34	98	<i>Mardecavirus</i> spp.
Pva1	Siphovirus (103, 72, 153, 9)	Linear 76 238	48.8	105	-	<a href="#">Vibrio phage vB_VpaS_HCMJ</a>	98.34	94	<i>Mardecavirus</i> spp.
Pva3	Siphovirus (59, 43, 157, 9)	Linear 76 161	48.8	103	-	<a href="#">Vibrio phage vB_VpS_C2</a>	97.17	96	<i>Mardecavirus</i> spp.
Pva7	Podovirus (51, 47, 8, 8)	Linear 41 749	44.4	117	-	<a href="#">Vibrio phage vB_ValP_VA-RY-3</a>	74.74	17	Unknown

hl: head length, hd: head diameter, tl: tail length, td: tail diameter, bp: base pairs, GC: Guanine-Citocine content, ORF: Open reading frame

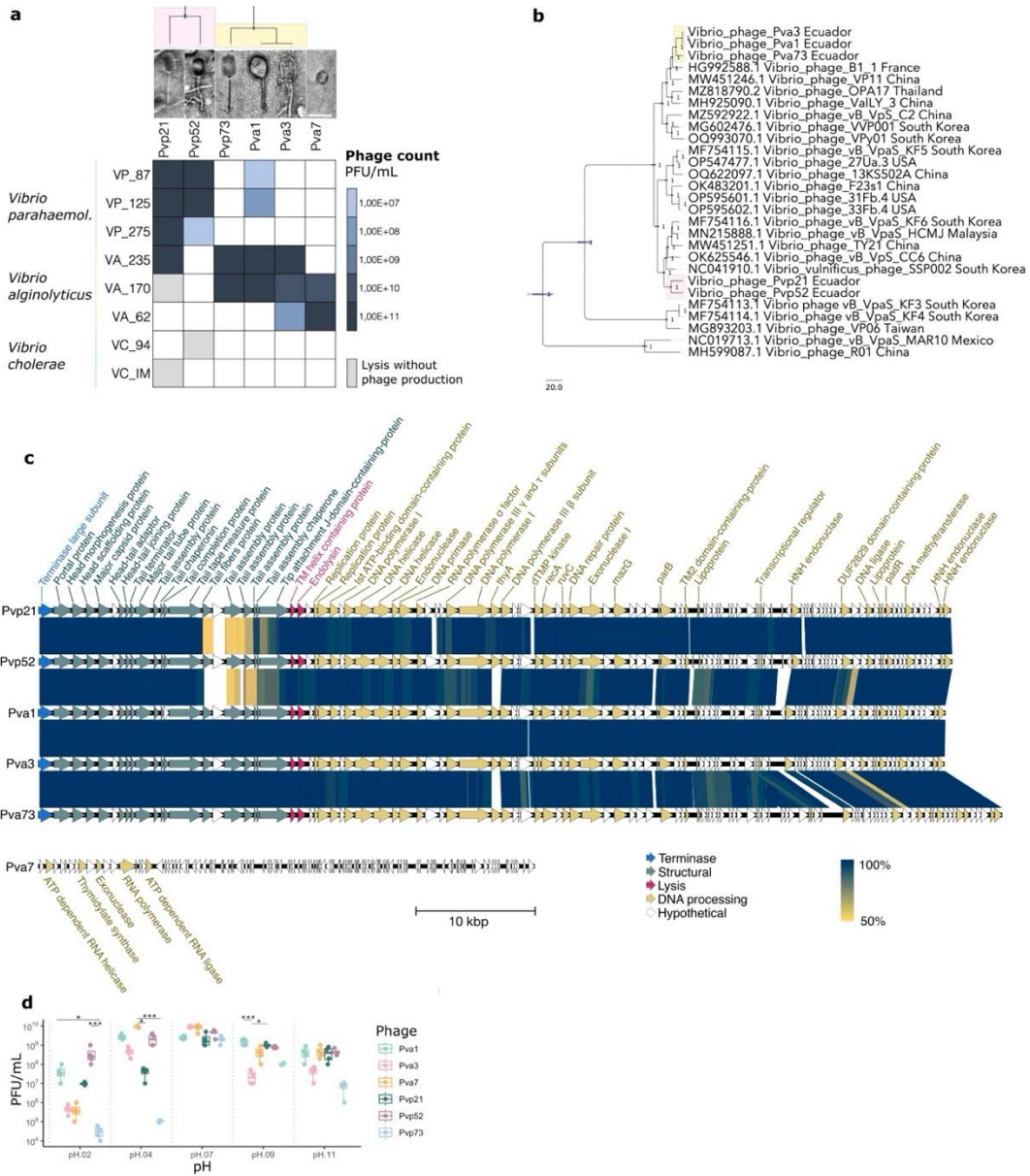


**Figure 1:** Phage infective, genomic, and stability characterization. **a.** Phage host-range and efficiency of plating in different hosts across three *Vibrio* spp. species. Phage titer in each host is shown in the simplified cross-interaction matrix, and the relative efficiency is shown as the color intensity of the interaction. TEM microphotographs of each phage are displayed for morphology comparisons. All phages are shown on the same scale, and the white line on Pva7 is calibrated to 100nm in length. **b.** MCC tree displaying phylogenetic relationships of our five Siphovirus with others from *Mardecavirus* spp. The phages isolated for this study are highlighted in yellow (mainly infecting *V. alginolyticus*) and in pink (mainly infecting *V. parahaemolyticus*). **c.** Genome annotations and comparative genomics of our six phages. Annotated genes have been classified into five categories, and the terminase gene was set as the starting point for the comparisons. Dark-grey blocs show the homology and the intensity of the color shows the conservation at the DNA sequence level of the phage genomes. Note that Pva7 has a shorter genome compared to the siphovirus and that only very few genes could be annotated due to the lack of homology to anything known. **d.** Phage counts of our six phages exposed to different pH conditions. Lines show significant differences in comparisons of phage viability within a pH value \*  $p < 0.05$ , \*\*  $p < 0.01$ , \*\*\*  $p < 0.001$ .

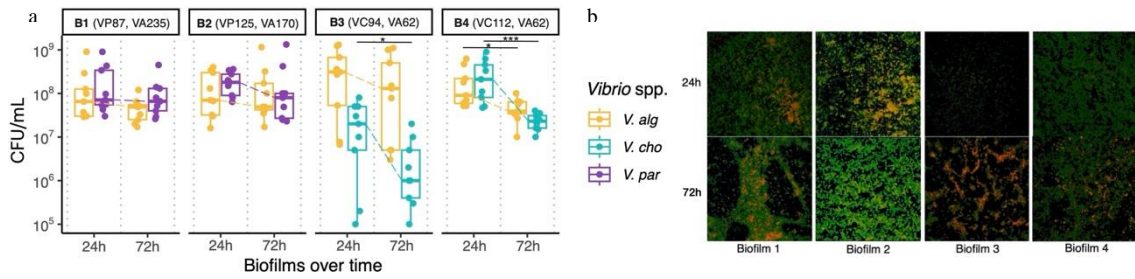


**Figure 2:** Preliminary characterization of dual-species biofilm of *Vibrio* spp. over time. a. Viability cell count of two biofilms of *V. parahaemolyticus* and *V. alginolyticus*, and two biofilms of *V. cholerae* and *V. alginolyticus*. Lines show significant differences in comparisons of phage viability within a biofilm \*  $p < 0.05$ , \*\* $p < 0.01$ , \*\*\* $p < 0.001$ . b. Fluorescent microscopy images of merged LIVE/Dead photographs of the biofilms.

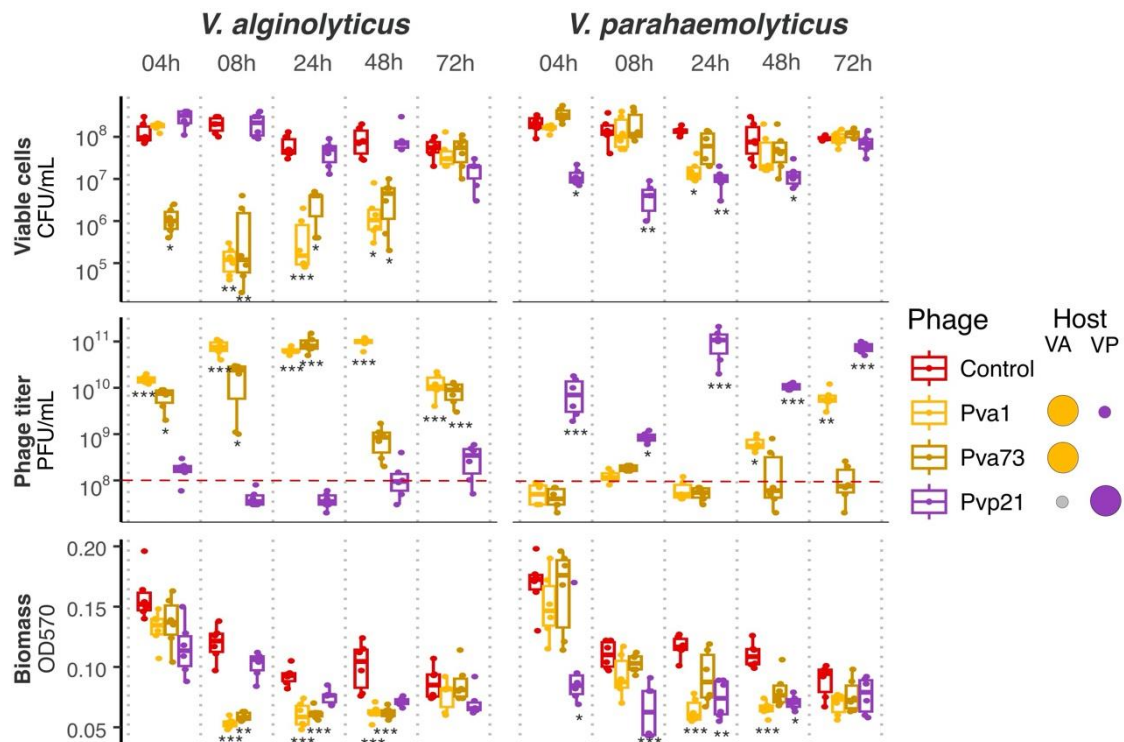


**Figure 3:** Effect of individual phages on single species biofilms of *V. alginolyticus* and *V. parahaemolyticus*. a. Viability cell count of individual bacteria exposed to each phage in a concentration of  $10^8$  PFU/mL roughly equivalent to a MOI of 1. Asterisk symbols under the boxplot show the significance of the comparison concerning the control without phage. \* $p < 0.05$ , \*\* $p < 0.01$ , \*\*\* $p < 0.001$ . b. Phage titer count (PFU/mL) of individual phages in *V. alginolyticus* and *V. parahaemolyticus* biofilms. Asterisks represent the significance level of the phage multiplication concerning the initial titer of  $10^8$  represented in the red dashed lines. c. Gross biofilm biomass measurement from the absorbance of suspended biofilms at 570 nanometers. Asterisks represent a significant effect concerning the control.

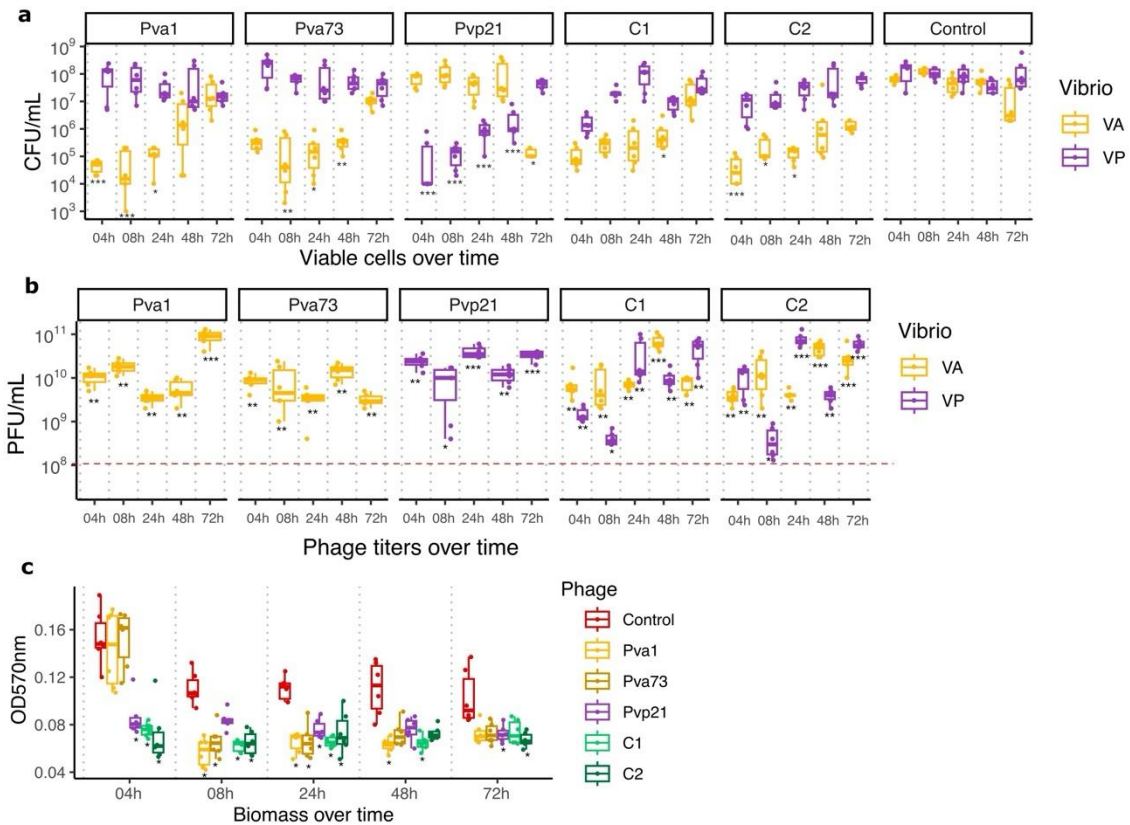


**Figure 4:** Effect of individual phages and phage cocktails on dual-species biofilms of *V. alginolyticus* and *V. parahaemolyticus*. a. Viability cell count of individual bacteria exposed to a total phage concentration of  $1e8$ . Phage cocktails contain a mix of C1) Pva1, Pvp21 and Pva73, and C2) Pva1, Pva3, Pva7, Pvp21, Pvp52 and Pva73. Phage cocktails contain an equal amount of each phage and a total amount of phages in solution of  $1e9$  ( $1e8$  once applied on biofilms). Asterisk symbols under the boxplot show the significance of the comparison concerning the control without phage at that time measurement \* $p < 0.05$ , \*\* $p < 0.01$ , \*\*\* $p < 0.001$ . Yellow boxplots represent counts of *V. alginolyticus* while purple boxplots represent *V. parahaemolyticus* counts. b. Phage titers count of phages in the biofilms over time. The dashed red line corresponds to the initial phage concentration applied. Asterisks represent significant respect to a  $1e8$  phage count. Yellow boxplots represent counts of phages for *V. alginolyticus* while purple boxplots represent counts for phages for *V. parahaemolyticus* c. Gross biofilm biomass measurement from the absorbance of suspended biofilms at 570 nanometers. Asterisks represent a significant effect concerning the control.

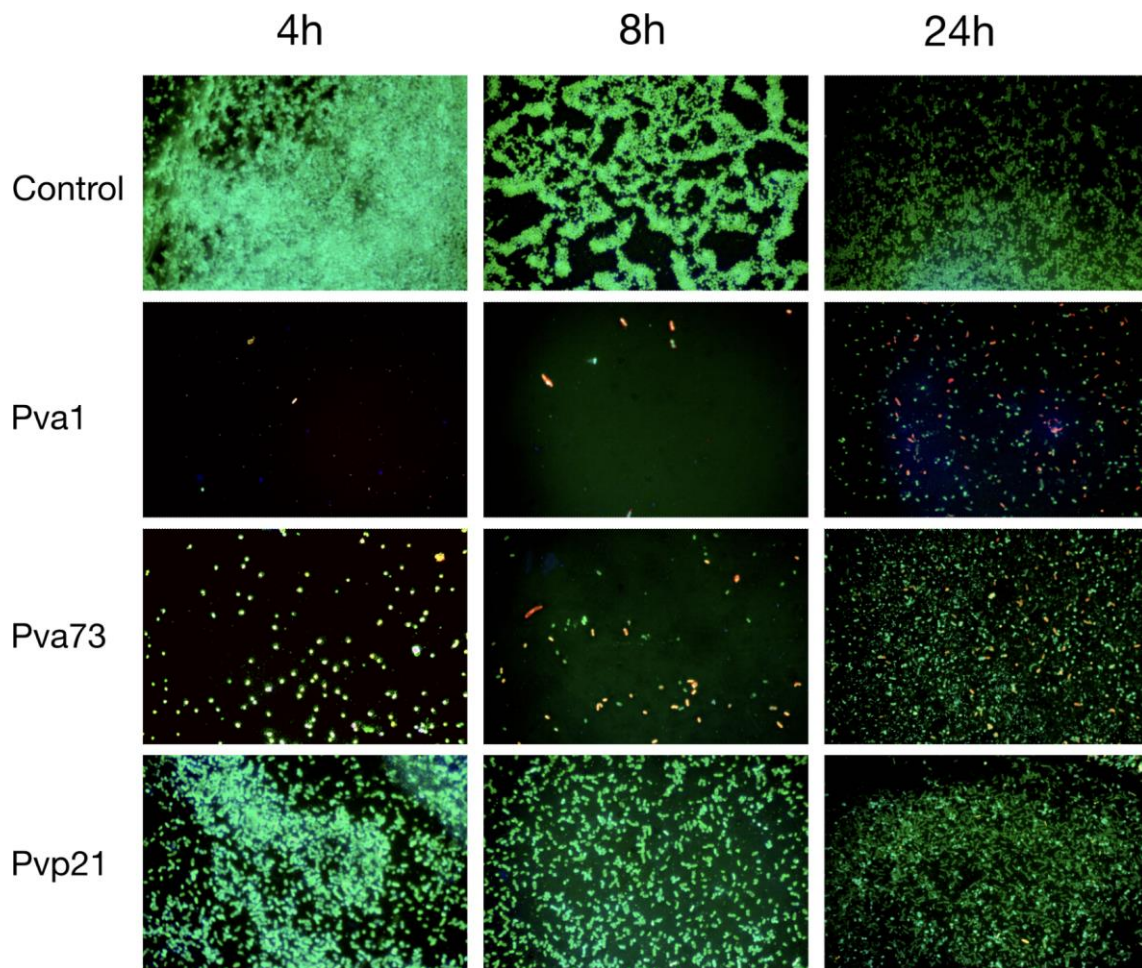


**Figure 5:** Fluorescence microscopy images of biofilms of *V. alginolyticus* formed over coverslip glass and challenged against 3 individual phages. Merged images using a Live/Dead fluorescent staining at a 1000X magnification are shown. Red cells correspond to dead cells while green correspond to live cells within the biofilm.

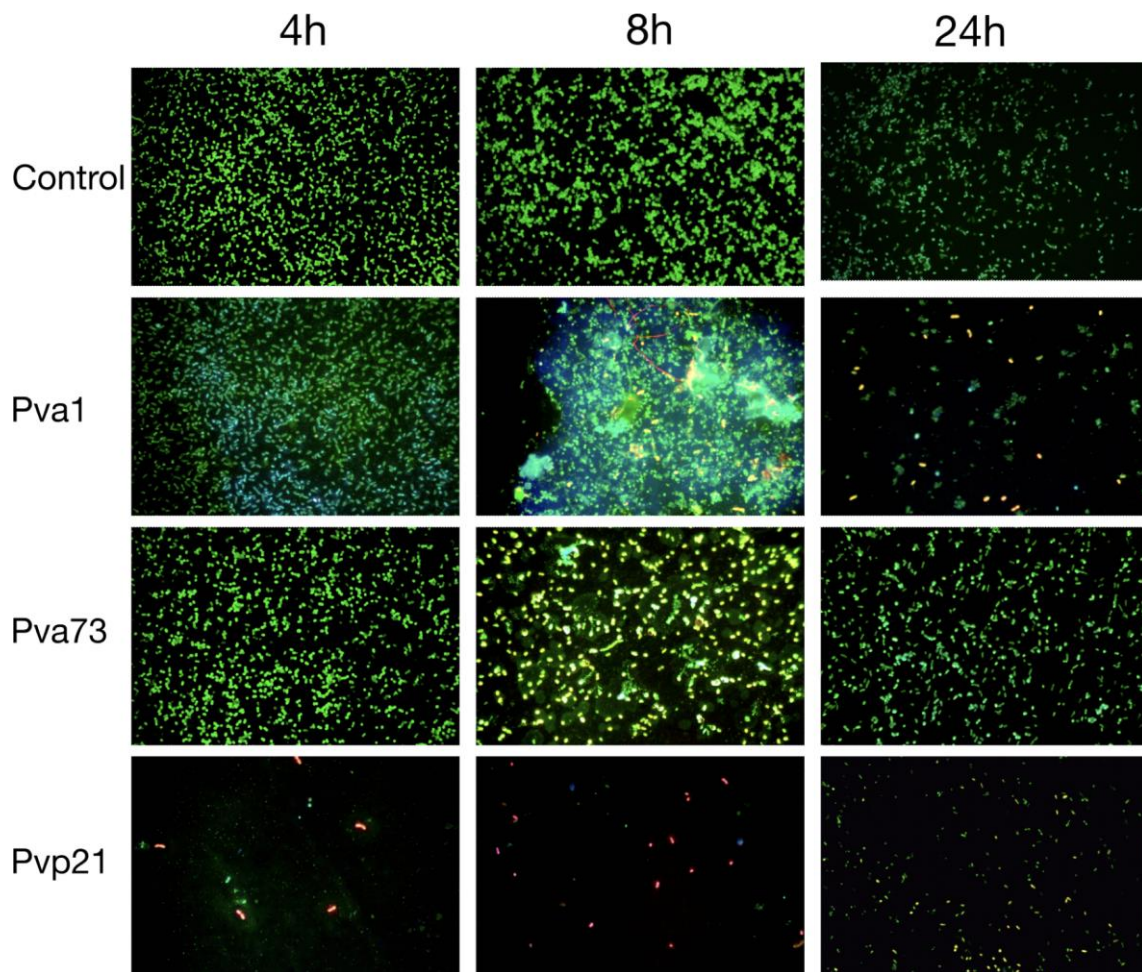


**Figure 6:** Fluorescence microscopy images of biofilms of *V. parahaemolyticus* formed over coverslip glass and challenged against 3 individual phages. Merged images using a Live/Dead fluorescent staining at a 1000X magnification are shown. Red cells correspond to dead cells while green correspond to live cells within the biofilm.

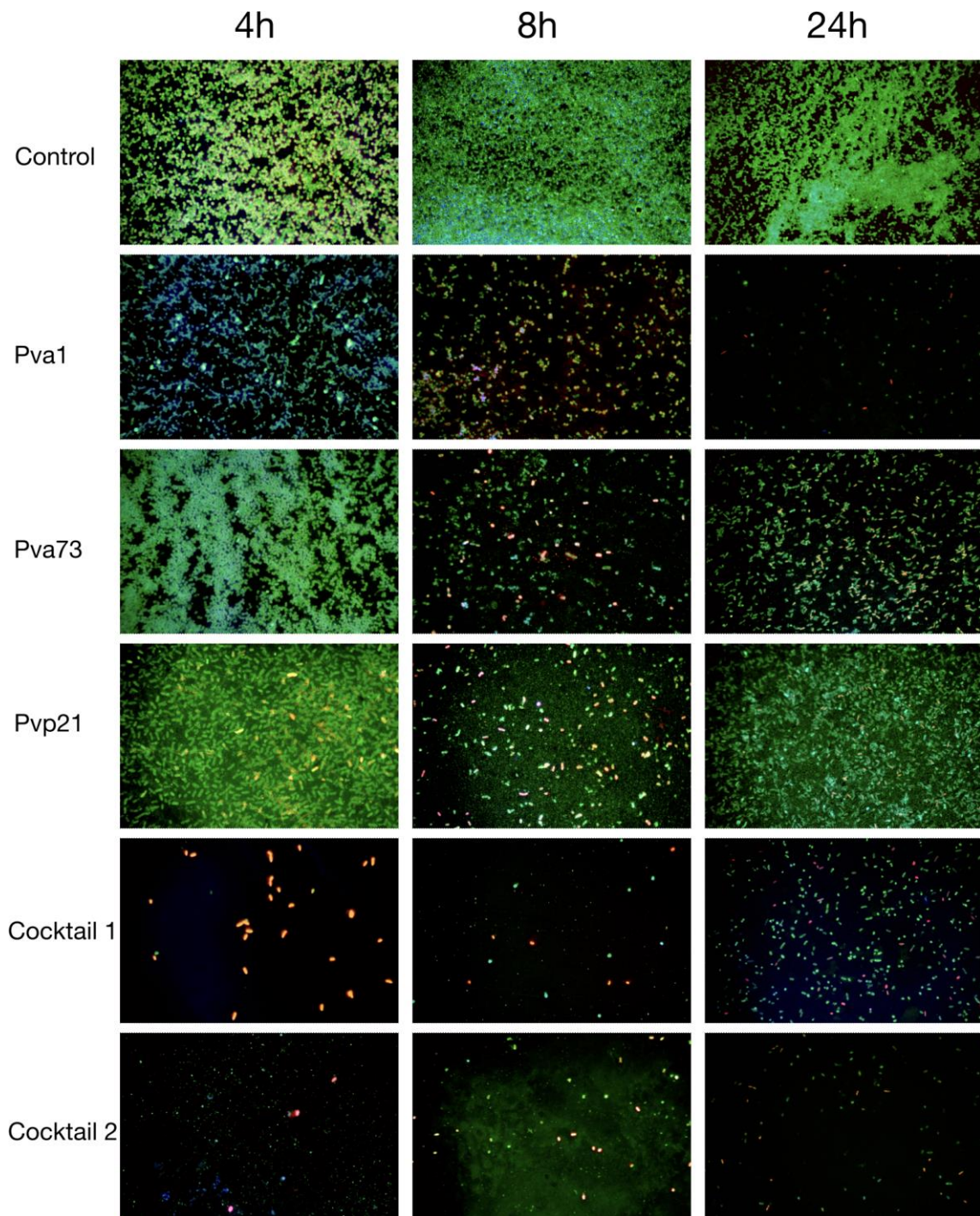


**Figure 7:** Fluorescence microscopy images of mixed biofilms of *V. alginolyticus* and *V. parahaemolyticus* formed over coverslip glass and challenged against 3 individual phages and 2 phage cocktails. Merged images using a Live/Dead fluorescent staining at a 1000X magnification are shown. Red cells correspond to dead cells while green correspond to live cells within the biofilm.



## ANEXOS / SUPPLEMENTARY INFORMATION

### ANEXO A: Antibiotic susceptibility test and biochemical results.

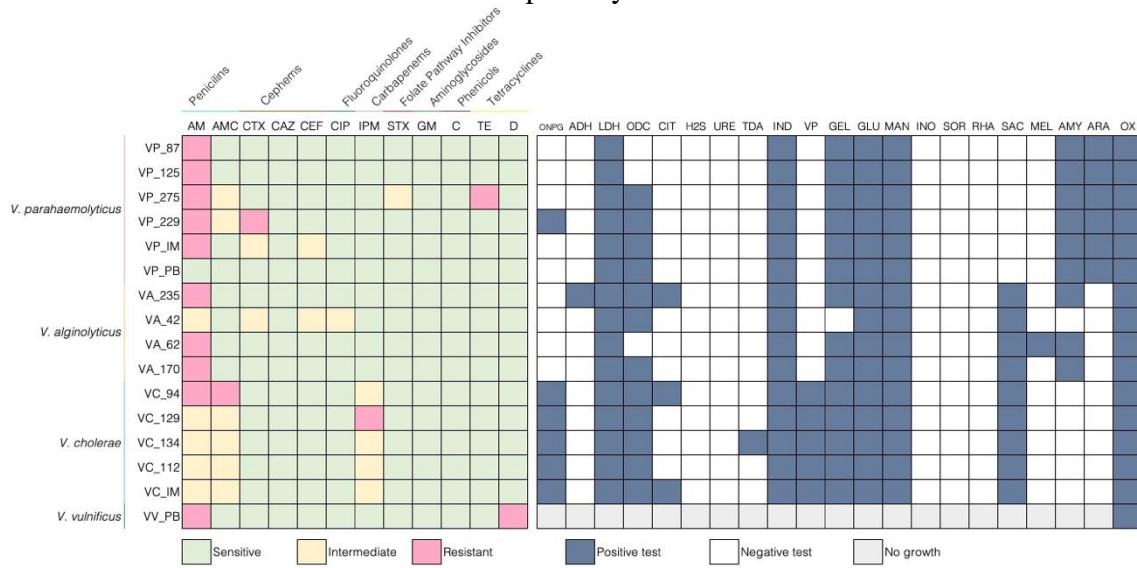


Figure S1: Antibiotic susceptibility test and biochemical results.

**ANEXO B:** Multiplex PCR for *Vibrio* species identification.

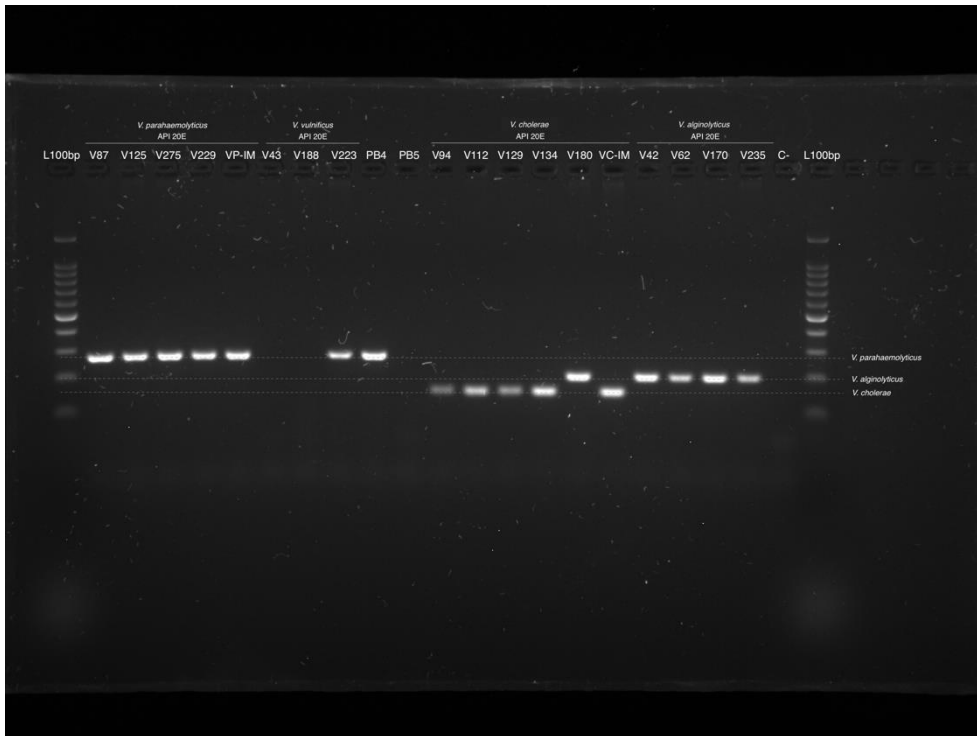


Figure S2: Agarose gel electrophoresis of multiplex PCR for *Vibrio* species identification.

## ANEXO C: Phage-*Vibrio* cross interactions from assay B.

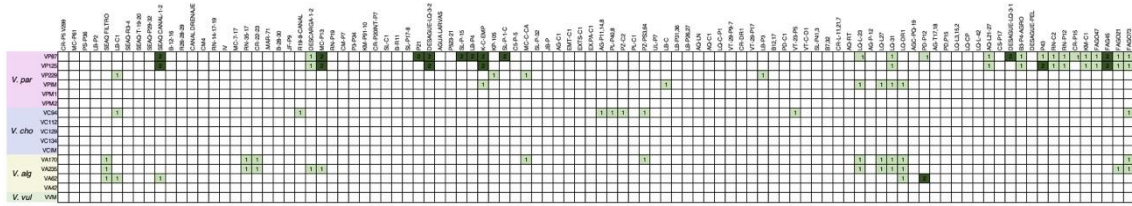


Figure S3: 1600 cross interactions of phage-positive solutions from “Assay B” against isolates of 4 *Vibrio* species.

**ANEXO D: Phage-*Vibrio* cross interaction matrix reflecting multiplication efficiency of phages in different hosts.**

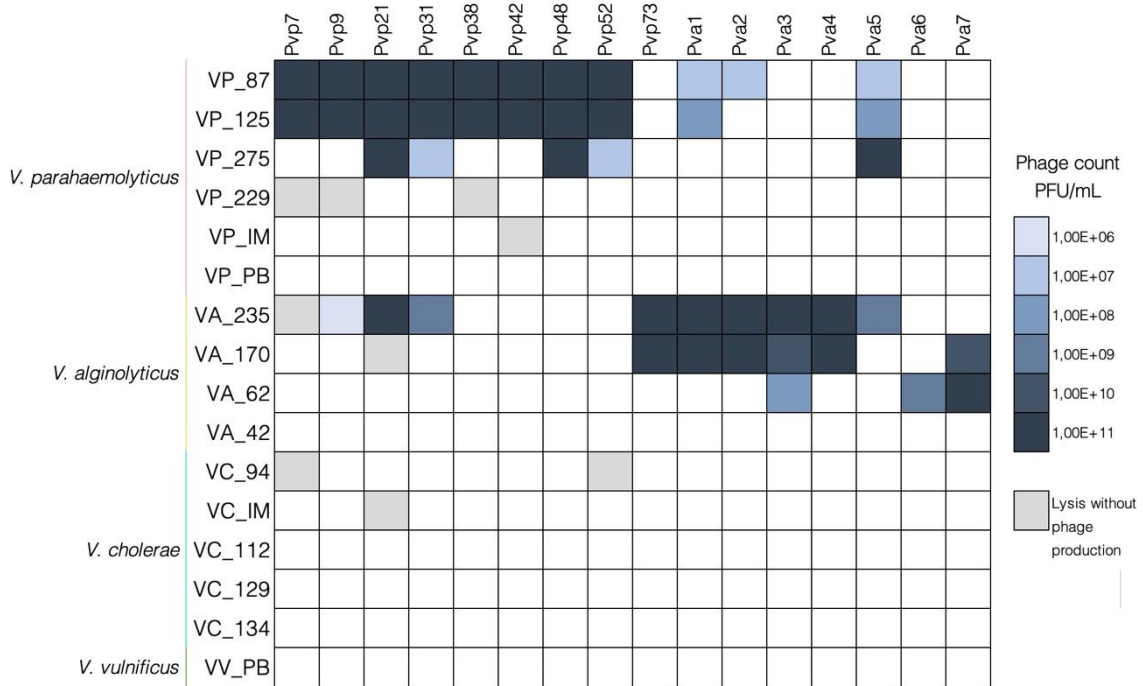


Figure S4: Complete cross-interaction matrix of the 16 phages with the best host range against the 16 diverse bacteria.

**ANEXO E: Transmission Electron Microscopy TEM microphotographs of ten isolated phages.**

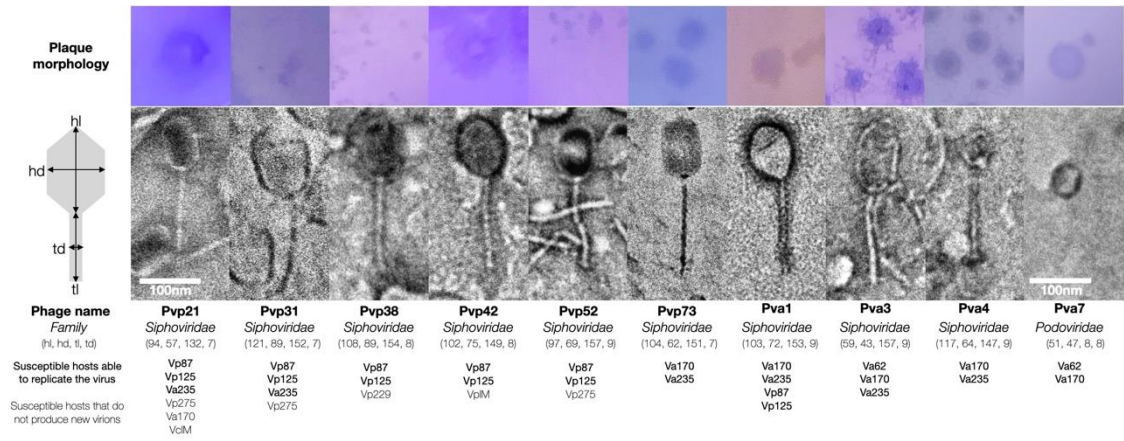


Figure S5: Phage morphological characterization using TEM analysis.

## ANEXO F: Comparative genomic analysis of *Mardecavirus* phages.

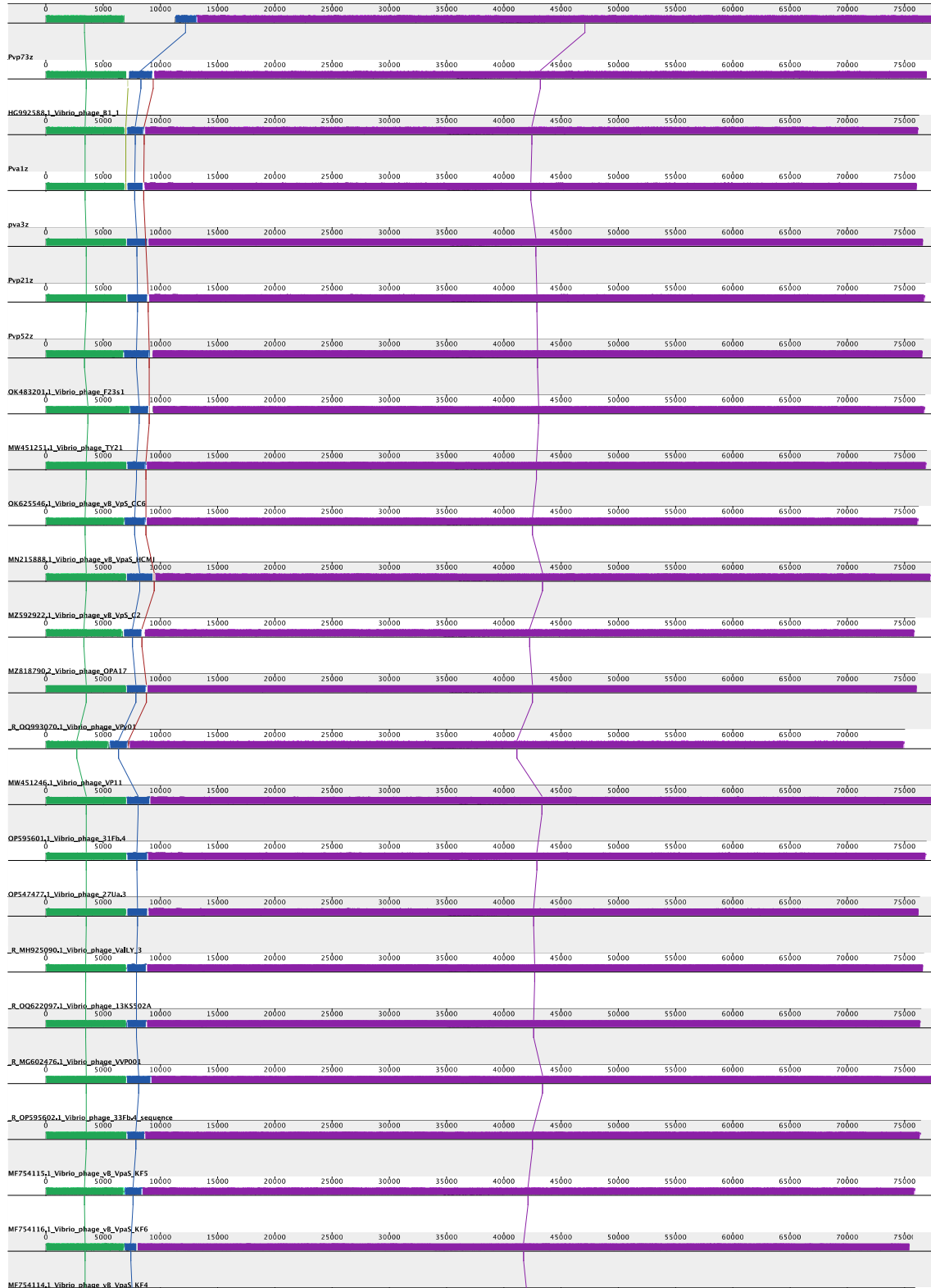


Figure S6: Evaluation of Multiple Genome Alignment analysis through processiveMauve software of *Mardecavirus* spp. phages' genomes.

**ANEXO G: GC-skew analysis of the six sequenced phages in this study.**



Figure S7: GC-skew and ORF directionality analysis of the six phage genomes.

**ANEXO H:** Fluorescence microscopy reflecting individual light channels and merged images of 4 dual-species biofilms.

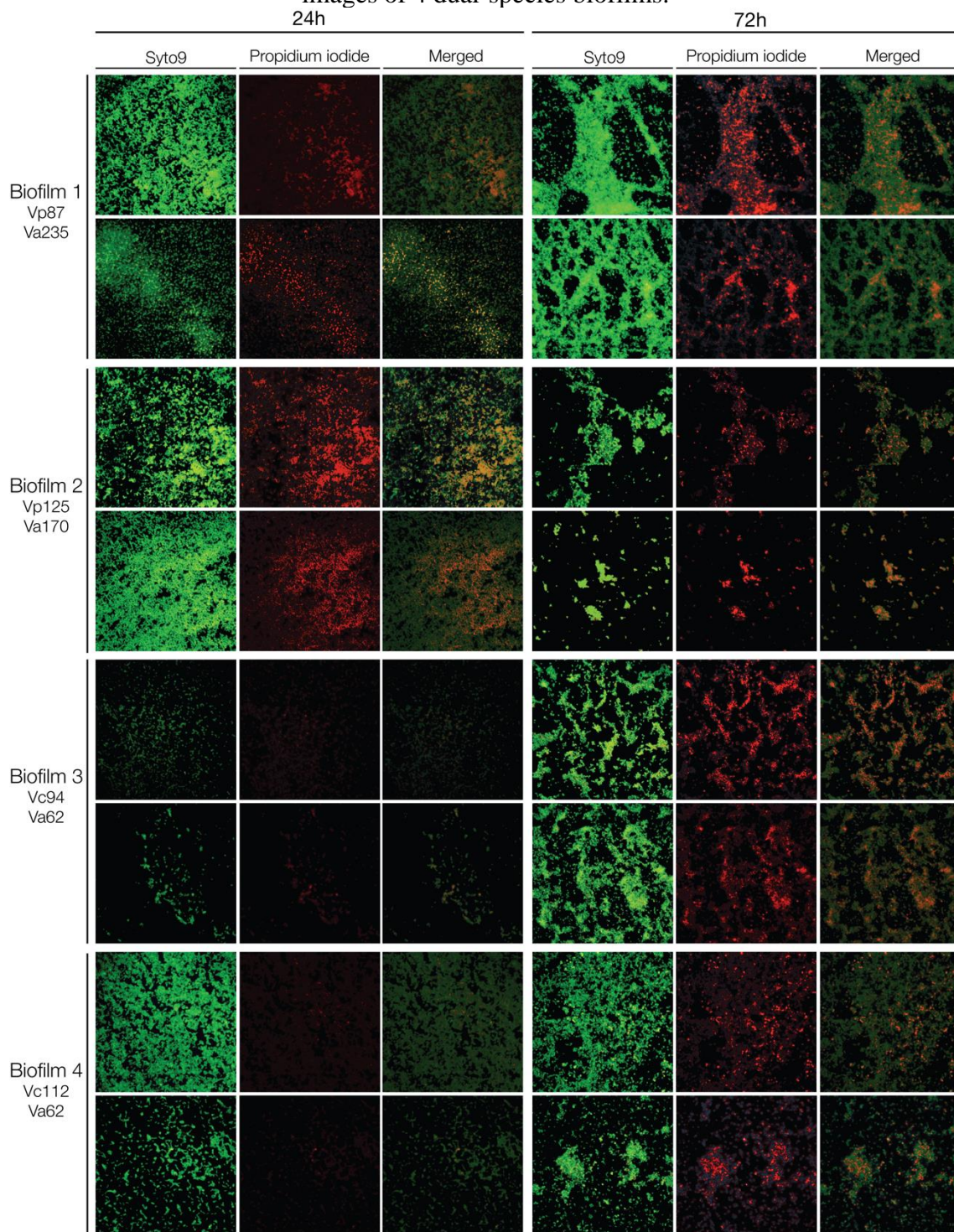


Figure S8: Live/Dead evaluation through fluorescence microscopy of dual-species biofilms at 24 and 72h.



**ANEXO I: Map of sampling sites.**

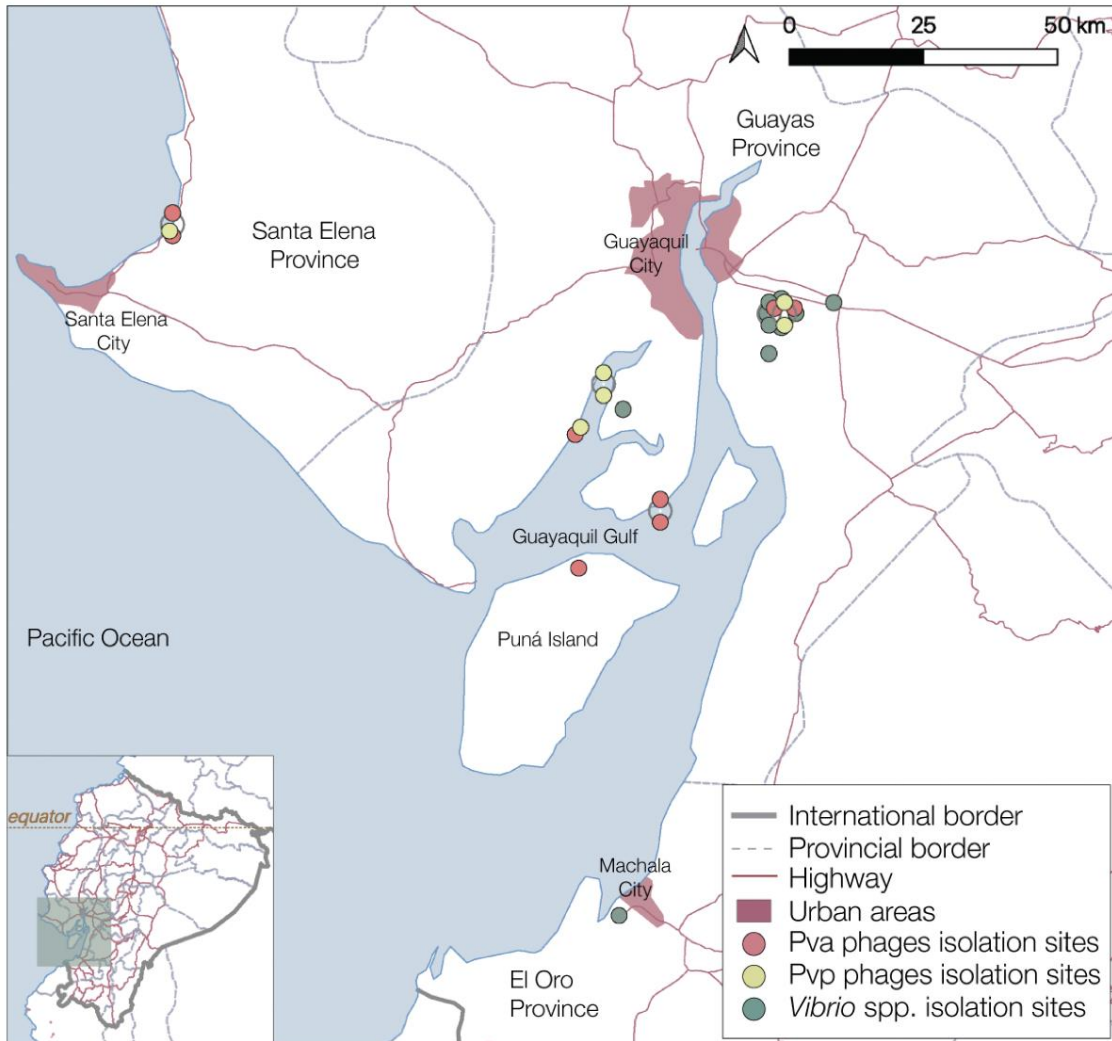


Figure S9: Illustration map of the sample collection of phages and bacteria obtained in the present study.

**ANEXO J: Summary of reagents, equipment, and resources mentioned in the Methods section (Supplementary Table 1).**

RESOURCE	ABREV.	SOURCE	CAT. NO.
<b>Bacteria and viruses</b>			
<i>Vibrio parahaemolyticus</i>	VP	Wildtype isolates	
<i>Vibrio alginolyticus</i>	VA	Wildtype isolates	
<i>Vibrio cholerae</i>	VC	Wildtype isolates	
<i>Vibrio vulnificus</i>	VV	Wildtype isolates	
Phages for <i>V. parahaemolyticus</i>	Pvp	Wildtype isolates	
Phages for <i>V. alginolyticus</i>	Pva	Wildtype isolates	
<b>Culture media</b>			
CHROMagarVibrio™		CHROMagar	VB912
BD DIFCO™ Thiosulfate Citrate Bile Sucrose Agar	TCBS	Becton, Dickinson, and Co.	265020
BD DIFCO™ Tryptic Soy Agar	TSA	Becton, Dickinson, and Co.	236950
BD BBL™ Tryptic Soy Broth	TSB	Becton, Dickinson, and Co.	292735
BD DIFCO™ Mueller Hinton Agar	MHA	Becton, Dickinson, and Co.	225250
BD DIFCO™ Mueller Hinton Broth	MHB	Becton, Dickinson, and Co.	275730
<b>Molecular biology reagents and kits</b>			
Oligonucleotides / Primers		Macrogen Co. (Table S2)	
DNeasy® Blood & Tissue Kit		Qiagen	69504
Qubit™ 1X dsDNA High Sensitivity Assay kit		Invitrogen	Q33231
SYBR Safe DNA Gel Stain		Invitrogen	S33102
Ultrapure™ EDTA		Invitrogen	15576028
Ultrapure™ Tris		Invitrogen	15504020
Boric Acid		Thermo Fisher Scientific	AAJ6720236
GoTaq® qPCR Master Mix		Promega	A6002
GoTaq® Flexi DNA Polymerase		Promega	M829A
5X Green GoTaq® Flexi Buffer		Promega	M891A
Magnesium chloride	MgCl <sub>2</sub>	Promega	A351B
dNTPs Mix 10mM		Promega	U1515
Agarose		Promega	V3125
100bp DNA Ladder		Promega	G2101
RNAse A solution		Promega	A7973
RQ1 RNAse Free DNase		Promega	M6101
Ethanol absolute grade			
<b>Reagents and kits miscellaneous</b>			
FilmTracer™ LIVE/DEAD™ Biofilm Viability Kit		Invitrogen	L10316
API® 20E strip tests		Biomérieux	20100
API® 20E reagents kit		Biomérieux	20120
McFarland Standards Kit		Biomérieux	70900
Mineral Oil		Biomérieux	70100
Phosphate Buffered Saline Tablets	PBS	Oxoid	BR0014G
Peptone special		Merck/Millipore	68971
Yeast extract		Merck/Sigma-Aldrich	Y1625
Potassium phosphate dibasic	K <sub>2</sub> HPO <sub>4</sub>	Merck/Sigma-Aldrich	P8181
Glycerol		Merck/Sigma-Aldrich	G5516
Immersion oil			
Sodium chloride	NaCl	AppliChem	131659
0.2 um Minisart® RC25 cellulose syringe filters		Sartorius	17764-----ACK
Ethanol 96%			
Methanol			
Cristal Violet Stain Powder	CV		
BD BACTO™ Agar		Becton, Dickinson, and Co.	214050
BD BBL™ Sensi-Disc™ Ampicillin	AM	Becton, Dickinson, and Co.	230705

<b>BD BBL™ Sensi-Disc™ Amoxicilin and Clavulanic Acid</b>	AMC	Becton, Dickinson, and Co.	231629
<b>BD BBL™ Sensi-Disc™ Cefotaxime</b>	CTX	Becton, Dickinson, and Co.	231606
<b>BD BBL™ Sensi-Disc™ Ceftazidime</b>	CAZ	Becton, Dickinson, and Co.	231632
<b>BD BBL™ Sensi-Disc™ Cefepime</b>	FEP	Becton, Dickinson, and Co.	231696
<b>BD BBL™ Sensi-Disc™ Ciprofloxacin</b>	CIP	Becton, Dickinson, and Co.	231657
<b>BD BBL™ Sensi-Disc™ Imipenem</b>	IMP	Becton, Dickinson, and Co.	231644
<b>BD BBL™ Sensi-Disc™ Trimethoprim/Sulfamethoxazole</b>	CXT	Becton, Dickinson, and Co.	231539
<b>BD BBL™ Sensi-Disc™ Gentamicin</b>	GM	Becton, Dickinson, and Co.	231227
<b>BD BBL™ Sensi-Disc™ Chloramphenicol</b>	C	Becton, Dickinson, and Co.	230733
<b>BD BBL™ Sensi-Disc™ Tetracycline</b>	TE	Becton, Dickinson, and Co.	230998
<b>BD BBL™ Sensi-Disc™ Doxycycline</b>	D	Becton, Dickinson, and Co.	231286
<b>Equipments</b>			
<b>Qubit 4 fluorometer</b>		Invitrogen	Q33238
<b>NanoDrop One Spectrophotometer</b>		Thermo Fischer Scientific	ND-ONEC-W
<b>GENESYS™ 20 Visible Spectrophotometer</b>		Thermo Fischer Scientific	4001000
<b>Water bath GP05</b>		Thermo Fischer Scientific	TSGP05
<b>T100 Thermal Cycler</b>		Bio-Rad Laboratories Inc.	1861096
<b>Molecular Imager® Gel Doc™ XR System</b>		Bio-Rad Laboratories Inc.	1708195EDU
<b>C1000 Touch Thermal Cycler</b>		Bio-Rad Laboratories Inc.	1851196
<b>CFX96 Touch Real-Time PCR Detection System</b>		Bio-Rad Laboratories Inc.	1845097
<b>Centrifuge 5804R</b>		Eppendorf	5805000010
<b>Centrifuge 5415D</b>		Eppendorf	EPP_5415D
<b>ENDURO Gel XL Electrophoresis system</b>		Labnet	E0160
<b>ZX4 Advanced IR Vortex Mixer</b>		VELP Scientifica Srl	F202A0280
<b>Compact Centrifuge Z206</b>		Hermle	Z206
<b>Olympus BX50 Fluorescence Microscope</b>		Olympus Optical Co. LTD.	BX50-FL-PA
<b>Elx808 incubating absorbance plate reader</b>		Agilent	BioTek Elx808
<b>Ultra-Low Temperature Mini Deep Freezer</b>		Biobase	Bdf-86V108
<b>Software and data analysis pipelines</b>			
<b>AMscope</b>			
<b>CellProfiler v4.2.5</b>			
<b>CellProfiler pipeline for cell count and viability estimations</b>		Deposited in: 10.6084/m9.figshare.24988 203	
<b>ImageJ v15.3k</b>			

**ANEXO K:** Primer sequences used throughout the study (Supplementary Table 2).

Target	Primer F sequence 5'-3'	Primer R sequence 5'-3'	Size bp	Ta °C	Ref.
<i>V. parahaemolyticus</i> collagenase gene	GAAAGTTGAACATCATCAGCACGA	GGTCMGAATCAAACGCCG	272	65	(Wei et al., 2014)
<i>V. alginolyticus</i> Core gDNA fragment	ACGGCATTGGAAATTGCGACTG	TACCYGTCTCACGAGCCCAAG	199	65	(H.-J. Kim et al., 2015)
<i>V. cholerae</i> Core gDNA fragment	CAAGCTCYGCATGTCCAGAAGC	GGGGCGTGACGCGAATGATT	154	65	(H.-J. Kim et al., 2015)
<i>V. vulnificus</i> <i>vvha</i> gene	ACTCAACTATCGTGCACGCTT	ACACTGTTCGACTGTGAG	367	65	(Neogi et al., 2010)

**ANEXO L:** Comparison of genome features and reported lifecycle of *Mardecavirus* spp. (Supplementary Table 3).

Phage name	NCBI Accession	Origin	Taxonomy ID	Host range	Genome bp	Config	%GC	ORF	Putative life cycle	Reference
Vibrio phage vB_VpaS_MAR10	NC_019713.1	Baja California, Mexico.	Mardecavirus MAR10	V. par	78 751	-	49.7	104	Temperate	(Alanis Villa et al., 2012)
Vibrio vulnificus phage SSP002	NC_041910.1	West sea, South Korea	Mardecavirus SSP002	V. vul	76 350	Linear	48.8	102	Possible transducing phage	(Lee et al., 2012)
Vibrio phage VVP001	MG602476.1	Yenpo, South Korea	Mardecavirus SSP002	V. vul	76 423		49.64	102	-	(H.-J. Kim et al., 2021)
Vibrio phage 27Ua.3	OP547477.1	Long Island, NY, USA	Unclassified Mardecavirus sp.	V. par	76 890	Linear	48.8	122	-	(Brossard Stoos et al., 2022)
Vibrio phage 31Fb.4	OP595601.1	Long Island, NY, USA	Unclassified Mardecavirus sp.	V. par	77 620	Linear	48.9	127	-	(Brossard Stoos et al., 2022)
Vibrio phage 33Fb.4	OP595602.1	Long Island, NY, USA	Unclassified Mardecavirus sp.	V. par	77 632	Linear	48.9	127	-	(Brossard Stoos et al., 2022)
Vibrio phage OPA17	MZ818790.2	Songkhla, Thailand	Unclassified Mardecavirus sp.	V. camp	75,897	Circular	48.41	102	Lytic	(Srisangthong et al., 2023)
Vibrio phage F23s1	OK483201.1	Wuhan, China	Unclassified Mardecavirus sp.	V. par	76,648	Linear	48.8	105	Lytic	(Xia et al., 2022)
Vibrio phage R01	MH599087.1	Dalian, China	Unclassified Mardecavirus sp.	V. par	75,514	Linear	49.42	75	Lytic	(Li et al., 2023)
Vibrio phage VP06	MG893203.1	Taiwan	Unclassified Mardecavirus sp.	V. par - V. alg	75,893	Linear	49	101	-	(Wong et al., 2019)
Vibrio phage KF3	MF754113.1	South Korea	Unclassified Mardecavirus sp.	V. par	75955	Linear	49	97	-	(Yu et al., 2018)
Vibrio phage KF4	MF754114.1	South Korea	Unclassified Mardecavirus sp.	V. par	75501	Linear	49	97	-	(Yu et al., 2018)

Legend: V. par: *V. parahaemolyticus*, V. vul: *V. vulnificus*, V. camp: *V. campbelli*, V. alg: *V. alginolyticus*, bp: base pairs, GC: Guanine-Citocine, ORF: Open reading frame.